GD/C-DBE-66-001a
Space Science Laboratory

STUDY ON EXHAUST PLUME RADIATION PREDICTIONS

INTERIM PROGRESS REPORT - PART II

FEBRUARY 1966

Technical Report

Research and Advanced Technology Department

CONTRACT NAS 8-11363

GENERAL DYNAMICS CONVAIR

GD/C-DBE-66-001a
Space Science Laboratory

STUDY ON EXHAUST PLUME RADIATION PREDICTIONS

INTERIM PROGRESS REPORT - PART II

FEBRUARY 1966

This work was sponsored by The George C. Marshall Space Flight Center of the National Aeronautics and Space Administration under Contract NAS 8-11363. The work was administered under the direction of the Aero-Astrodynamics Laboratory (R-AERO-R) of The George C. Marshall Space Flight Center of Huntsville, Alabama.

GENERAL DYNAMICS CONVAIR

TABLE OF CONTENTS

I. Introduction

In this section of the Interim Progress Report we complete the description of the work carried out during the past year on the analytic heat transfer studies portion of this contract. In Part I of this report five subjects were covered:

1) a summary of the presently available "best" values of the absorption coefficients for CO_2, H_2O, and CO;
2) a summary of the procedures used to evaluate these coefficients and preliminary estimates of the fine structure parameters for water vapor;
3) an analysis of the 1/S intensity distribution function and corresponding curves of growth with application to CO_2;
4) calculations of the high pressure limit for the total emissivity of water vapor versus temperature and pathlength; and
5) a brief description of the inhomogeneous gas radiance calculation.

In the present Part II, work carried out in the following areas is described:

1) representations of the curves of growth that are useful at low pressures (Doppler broadening) and for inhomogeneous gases;
2) evaluation of the line intensity and line spacing parameters for CO_2 from Malkmus' weak and strong line calculations;
3) sensitivity of the inhomogeneous radiance calculation to approximations made in the descriptions of the "hot" and

"cold" lines and to the choice of the intensity distribution functions;

4) line half widths of H_2O, CO_2, and CO;

5) detailed description of the current inhomogeneous radiance calculation (Model 3 and 3a).

These methods and data have been developed during the last several years under a continuing program on infrared radiative transfer from high temperature gases. In addition to company sponsored studies, the studies have been supported in large part by ARPA under Project DEFENDER, and more recently by NASA (MSFC). The principal objective of the ARPA program is the development of theoretical models of the infrared radiative properties of missile exhaust plumes for the purpose of long range detection. The radiative transfer studies have been divided into three principal areas: the experimental determination of the absorption coefficients of various molecules, the theoretical calculation of the spectral emissivities in the thin, square root, and Doppler limits, and the development of a practical calculation procedure that can be applied to gas volumes having arbitrary pressure, composition and temperature profiles. Since the ARPA study has been primarily concerned with the development of approximate overall exhaust plume models, detailed sensitivity analyses and assessments of the accuracy of the radiative transfer techniques has not been of major concern in this study. In general, the objective has been to develop techniques that are reliable to within about a factor of 2.

The NASA study has a similar objective but the requirements on accuracy and assessment of reliability are considerably higher. Also, the optical depths involved are considerably greater. The NASA effort

has had and does have four principal objectives:

1) the measurement of absorption coefficients for clouds of small carbon particles and the comparison of these with the theoretical models developed previously;

2) refinement and assessment of the accuracy of the molecular absorption coefficients for H_2O, CO_2, and CO which have been and are being evaluated in experimental and theoretical studies conducted under the ARPA program. Of principal importance here are analyses to determine the sensitivity of the total radiative heat transfer from homogeneous and inhomogeneous gas volumes to the inherent uncertainties in the measured spectral absorption coefficients and to establish a quantitative measure of the reliability of such calculations;

3) continuing development and refinement of the formalism for calculating the radiance of homogeneous and inhomogeneous gas volumes. Included in this area are sensitivity analyses to determine the errors resulting from various approximate curve of growth representations, line width and shape representations, rotational fine structure representations, and the use of the modified Curtis-Godson approximation;

4) experimental determination of the fine structure parameters for H_2O from long path high temperature measurements at various pressures in the long burner. These measurements will be used to test and refine the curve of growth and

fine structure formalism and to yield values for the line width to line spacing parameters as a function of temperature and wavenumber.

Because of the obvious close interdependence of these programs, it is both difficult and undesirable to maintain a clear division between the two studies. In general the ARPA work has been concerned with the experimental and theoretical determination of the molecular emissivities in the weak line limit (i.e., the absorption coefficients) and theoretical calculations of the Lorentz strong line limit (square root region) and of the Doppler strong line limit (very low pressure). Also methods for evaluating the radiance of inhomogeneous gases have been developed under this study.

To date the NASA effort has been directed towards an experimental determination of carbon absorption coefficients, sensitivity analyses for and refinements of the fine structure, line width, curve of growth representations, and of the inhomogeneous radiance calculation. Thus items numbered 1, 2, and 5 describing the work reported in Part I of this progress report (see page 1 of this section), represent the results of rather extensive studies carried out principally under the ARPA contracts, although the summarizing, tabulation, and presentation of this data was supported in part by both agencies. Also items 1 and 5 belonging to Part II (see page 1) represent summaries of work carried out principally under the ARPA contracts. Although some of this data has been previously reported under the ARPA contract, we have felt it desirable to include a fairly detailed description of all these areas in the present progress report.

In the future, in order to keep these studies distinct so that credit

may be assigned in an appropriate manner, we will maintain the following formal separation: the ARPA studies are associated with the initial determination of the molecular absorption coefficients and the initial development of the curves of growth and fine structure representations and the inhomogeneous gas calculational procedures; the NASA studies are responsible for the sensitivity analyses, assessments of accuracy and calculational efficiency, refinements of the curve of growth, line width, and fine structure representations and for the empirical determination of the fine structure parameters for water vapor in the long burner measurements. However, since for technical reporting purposes such a distinction would be totally impractical, mutual credit will be given to both agencies when the data to be described is a result of a significant amount of effort in each area. Primary emphasis will be given to producing the most useful technical documents.

In the following sections II and III of this report, we discuss the curve of growth and fine structure representations, the grouping of "hot" and "cold" lines, and the sensitivity of the inhomogeneous radiance calculation to the details of the formalism. In Section IV the line widths of H_2O, CO_2, and CO are discussed and in Section V a detailed description of the current radiance calculation is given (this is denoted Model 3). Also in Section V a simplified form (Model 3a) is described. Four radiance models currently exist (1, 2, 3, 3a). Model 1 is a preliminary model developed some time ago and has never been formally reported in detail. An informal description of this model was given to the contract monitor previously. Model 2 (which applies to only H_2O in the non-Doppler broadened region) was described in Part I of this progress report. This model is

a simpler model for homogeneous gases which groups all the lines together in a single curve of growth [Eq. (5)] and was used as the model for deducing H_2O absorption coefficients from empirical data obtained by various investigators. Model 3 is an improvement of Model 1 and represents our current "best" method for evaluating the infrared radiance of gases containing CO_2, H_2O, CO, H_2, N_2, O_2, and carbon which have arbitrary temperature, composition, and pressure profiles. Model 3a is a simplified version of Model 3 which does not distinguish between "hot" and "cold" lines. For homogeneous gas volumes containing H_2O only at pressures greater than 0.1 atmosphere (for which Model 2 is applicable), Models 3 and 3a are somewhat different from Model 2 (see Figs. 18 and 19) but the differences are within the present experimental uncertainties.

II. Curves of Growth and the Determination of the Fine Structure Parameters

In the random or statistical band model, the transmission function $(\bar{t})$ may be written as a product of the transmissions t_i of the individual line sequences which result from transitions having different upper vibrational states:

$$\bar{t} = \prod_i \bar{t}_i \tag{1}$$

In Fig. 1 we show a schematic breakdown of the CO_2 spectrum into individual sequences. Here $\bar{t}_i$ is related to the ratio of the mean equivalent width W_i to the mean line spacing d_i of the ith sequence:

$$\bar{t}_i = \exp(-W_i/d_i) \tag{2}$$

It is convenient to express the ratio $(W/d)_i$ in terms of the smeared absorption coefficient $\bar{k}_i$ $(= S_i/d_i)$ and the ratio a_i of the line half width to mean line separation $(a_i = \gamma_i/d_i)$:

$$(W/d)_i = a_i \, f(\bar{k}_i u/a_i) \tag{3}$$

Here u is the pathlength. The dimensionless function f(x) is the curve of growth for the ith sequence. For equally intense randomly distributed Lorentz lines, $2\pi f(x/2\pi)$ is the Ladenburg-Reiche function:

$$\underset{LR}{f(x)} = xe^{-x/2\pi}\left(J_o\left(\frac{ix}{2\pi}\right) - iJ_1\left(\frac{ix}{2\pi}\right)\right) \tag{4}$$

Within 10% this function may be approximated by the somewhat simpler form (see Fig. 2a):

$$f_1(x) = x/\sqrt{1 + x/4} \; . \tag{5}$$

This curve of growth is exact for an exponential distribution.

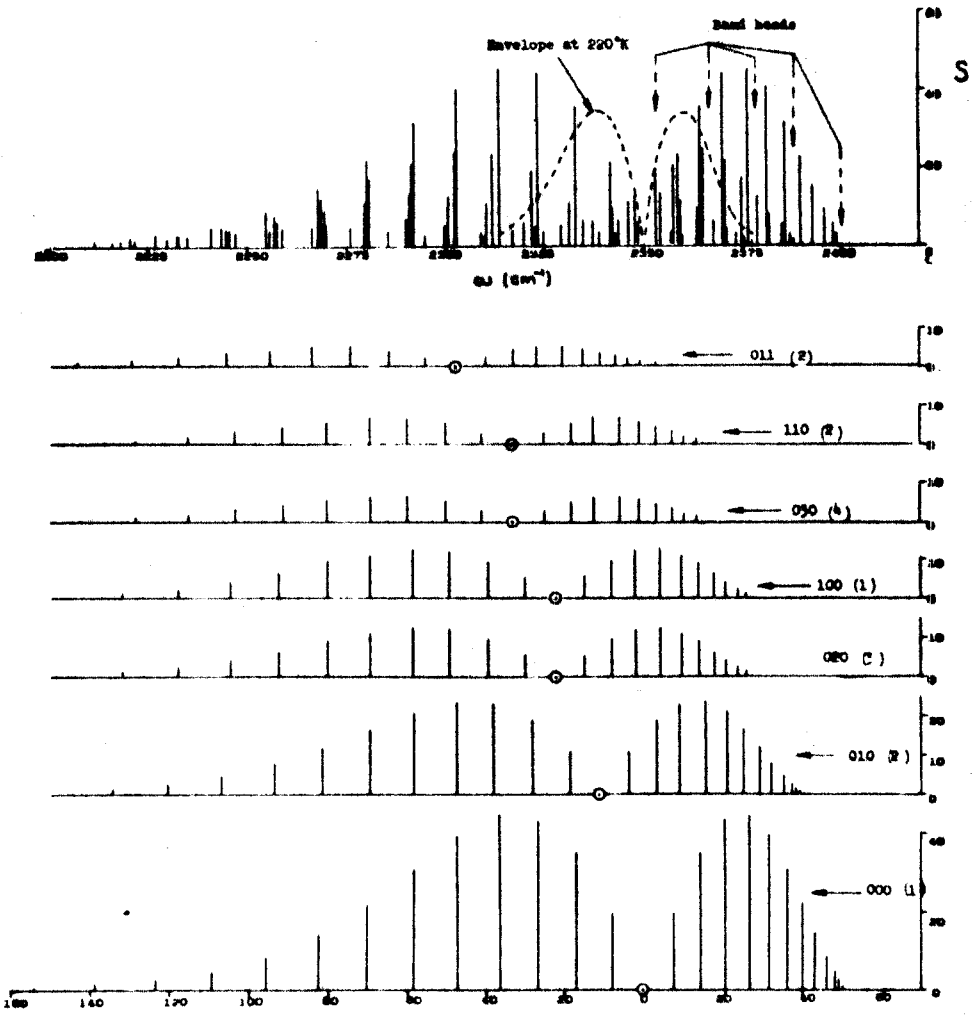

Fig. 1. Partial representation of the line intensities of CO_2 at 1500°K. The total spectrum is a superposition of a number of individual sequences or branches corresponding to transitions between different vibrational levels (of which only a few are shown). The lower state of the transition is denoted by vibrational quantum numbers (v_1, v_2, v_3) to the right of each sequence. The bracketed value is the number of sequences which have the same values of v_1, v_2, v_3 in the lower state. For clarity every fifth rotational line is shown only.

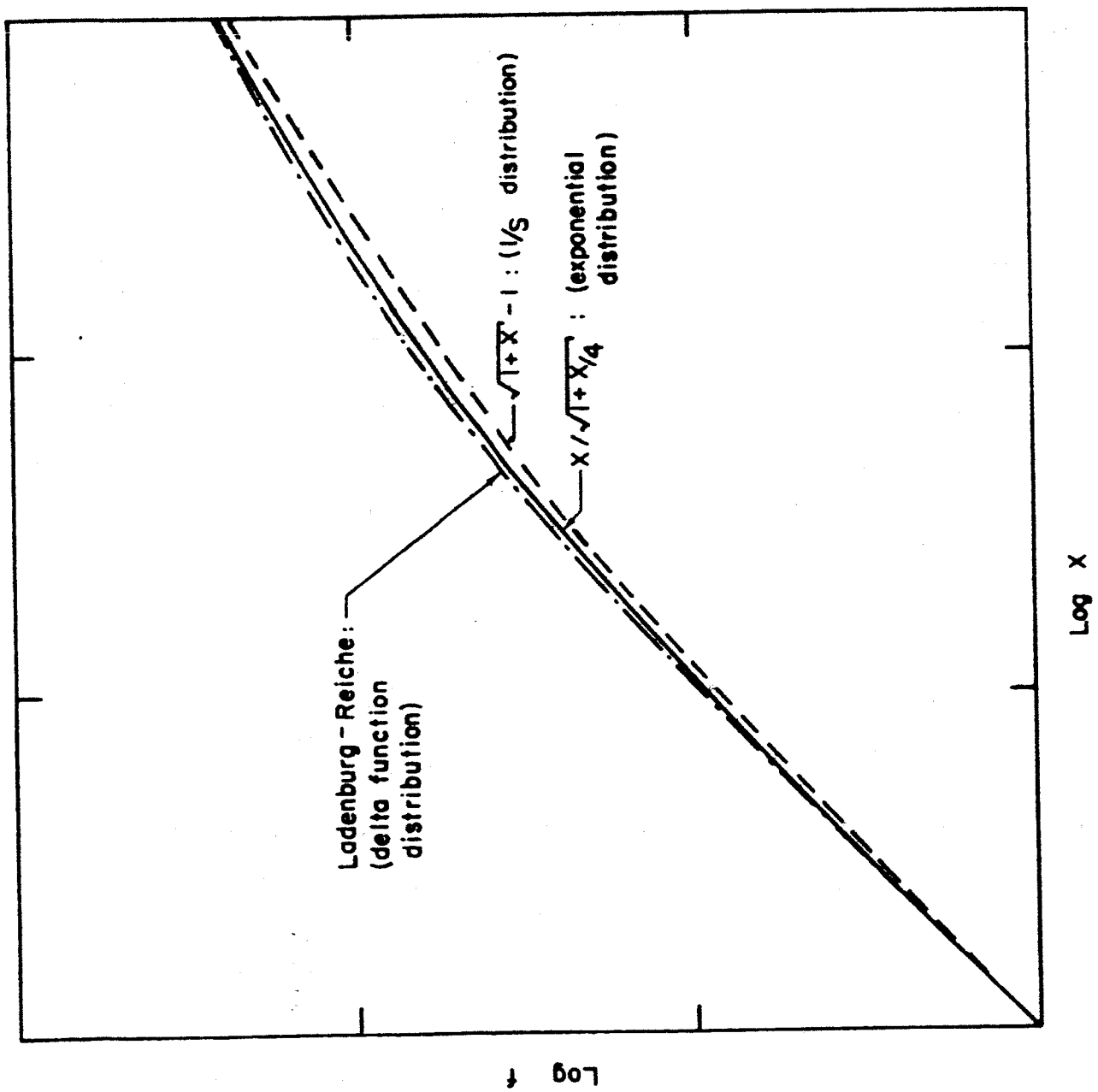

Fig. 2a. Collision broadened curves of growth for various intensity distributions.

No simple functional relation exists for equally intense Doppler lines. However, for most purposes the following representation is adequate (within 10% - see Fig. 2b):

$$f_2(x) = 1.7\sqrt{\ln\left(1+(.589x)^2\right)} \tag{6}$$

When the total number of branches contributing to the emission at a particular wavelength is relatively small and not too many evaluations of $\bar{t}$ are required, it is feasible to compute the contribution ($\bar{t}_i$) from each fundamental sequence individually and multiply the individual terms together. However, for polyatomic molecules such as CO_2 and H_2O at high temperatures this is usually too complex in practical situations, particularly for inhomogeneous nonisothermal mixtures. Here it is desirable to separate the contributing lines into a relatively small number of groups each of which can be treated in terms of a single curve of growth. The simplest method is to assign all the lines to one group and approximate the curve of growth by a single universal temperature and pressure independent function, such as the Ladenburg-Reiche function or that corresponding to an exponential or 1/S intensity distribution. In this approximation the transmission properties can be specified in terms of two parameters at each wavelength and temperature: the mean absorption coefficient $\bar{k}$ and the mean value of the line width to spacing ratio $\bar{a}$. For homogeneous gases at high pressures where Doppler broadening is not important, this has been found to yield reasonably accurate results when the line spacing is chosen so that the correct limiting values are obtained in the square root region. This is due to the fact that, for Lorentz lines, the curves of growth are relatively insensitive to the intensity

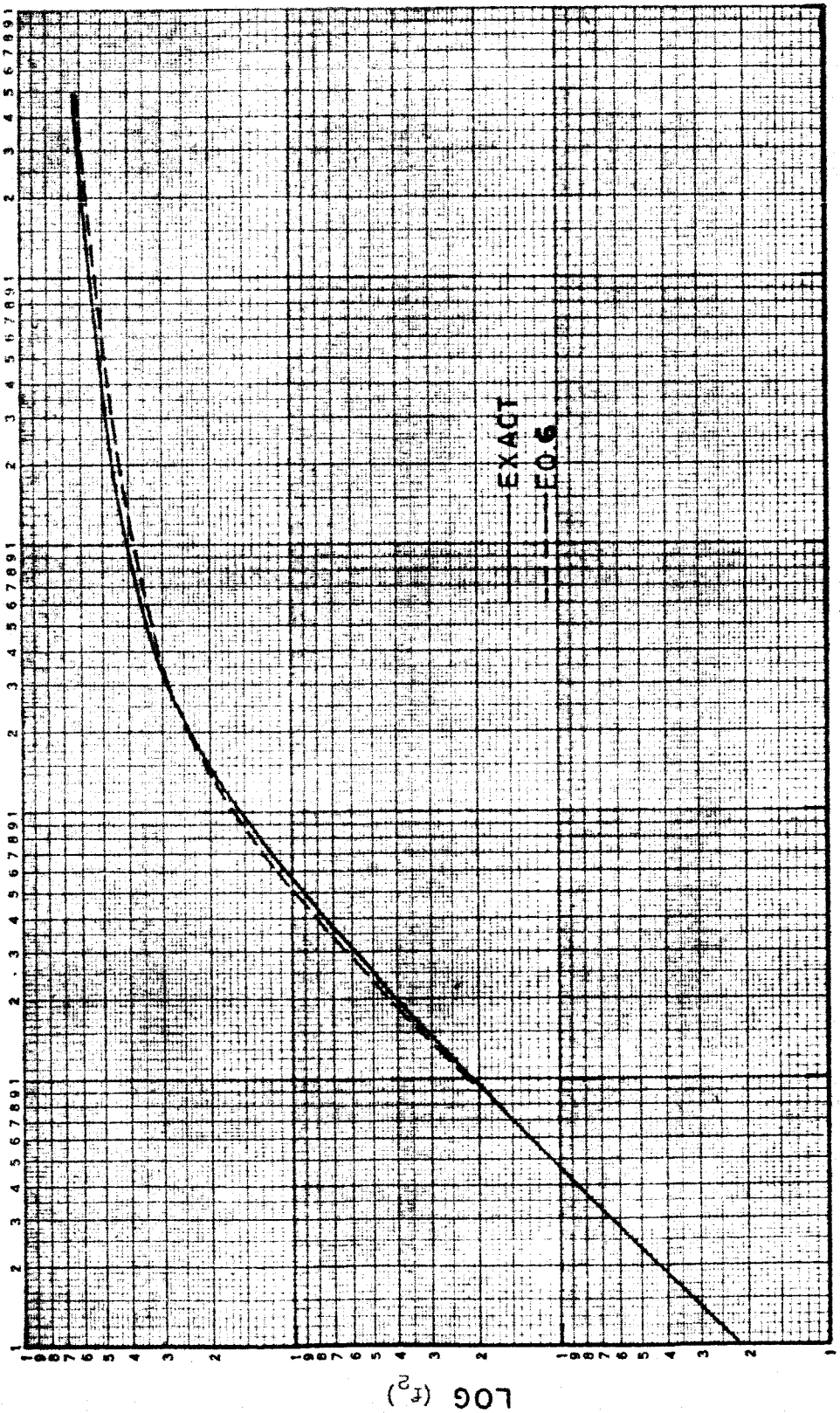

Fig. 2b. Doppler broadened curve of growth.

distribution functions. For example, the curve of growth for a delta function distribution ($\delta(S-\bar{S})$) differs from that for a $1/S\ e^{-S/\bar{S}}$ distribution by less than 25% throughout the entire range of optical depth.(see Fig. 2a).

However, when Doppler broadening is important or when treating inhomogeneous gases in the Curtis-Godson approximation, the errors resulting from this approach can be serious in some situations. When Doppler broadening is dominant, a more accurate accounting of the weaker lines is required when dealing with optically thick systems. In a nonisothermal gas in which a hot interior is surrounded by a cool absorbing exterior, this two-parameter approximation tends to overestimate the attenuation of the cool outer gas for the radiation emitted by the "hot" lines in the high temperature interior region. Since, in general, the "hot" lines tend also to be the lower intensity lines, both of these problems can be alleviated by separating the lines into groups according to their dependence on temperature.

The intensity of an individual spectral line, which lies in the spectral interval between ν and $\nu + \Delta\nu$, may be expressed in a general form which exhibits the dependence on temperature and quantum numbers of the particular transition:

$$S_i = \frac{\rho\ h(v_i, J_i)}{\Psi(T)}\ e^{-E_i/kT} \qquad (7)$$

Here v_i and J_i represent the group of quantum numbers required to specify the transition, E_i is the energy of the upper state, ρ is the density of the species and $\Psi(T)$ a function dependent only on temperature. Except for the factor $\rho/\Psi(T)$, which is common to all the contributing lines, the only temperature dependent factor is the exponential term. We may thus group the lines according to the value of E_i. If the energy scale is divided into equal

intervals of width ΔE, the ith line is to be assigned to the nth group if $(n-\frac{1}{2})\Delta E < E_i < (n+\frac{1}{2})\Delta E$. Thus the mean absorption coefficient for the nth group $(\bar{k}_n = (\bar{S}/d)_n)$ is given by

$$\bar{k}_n = \frac{N_n}{\Delta\nu} \sum_i \left[\frac{p}{Y} h(v_i, J_i)\, e^{-(E_i - n\Delta E)/kT}\right] e^{-n\Delta E/kT} \qquad (8)$$

where the sum is to be carried out over lines (N_n in all) which fall in the interval $\Delta\nu$ and for which $|E_i - n\Delta E| \leq \Delta E/2$. The mean line density $(\frac{1}{d_n})$ for this group is $N_n/\Delta\nu$. These expressions may be rewritten in the form

$$\frac{1}{d_n} = g_n/d_o$$

$$\bar{k}_n = \bar{k}(T)\, f_n\, e^{-n\Delta E/kT}/Q(T) \qquad (9)$$

where $Q(T) = \sum_{n=0}^{\infty} f_n\, e^{-n\Delta E/kT}$, $f_o \equiv 1$ and $g_o \equiv 1$. Thus $\bar{k}(T)$ is the local total absorption coefficient in the just overlapping line approximation. This is a convenient representation since the results (i.e., radiancies) tend to be relatively insensitive both to the values of f_n and g_n and to the value of ΔE. The value of ΔE should be chosen as large as possible commensurate with the requirement that the coefficients f_n may be approximated by temperature independent values. A convenient choice for ΔE is the energy of the least energetic vibrational mode of the molecule. Having chosen a value for ΔE, the values of f_n and g_n may be determined from a detailed theoretical calculation at representative temperatures when these are

available. Very often, however, either the theoretical calculations are not available or are not as accurate as available experimental data. When the linear (weak line) and the square root (strong line) limits are available from experiment, the theoretical calculations may be used to choose values for the g_n and f_n, for which high accuracy is not important, and the experimental data to derive values for the more sensitive parameters $\bar{k}$ and d_o. The linear portion of the curve of growth yields the value of $\bar{k}$ directly. In the square root region, the log of the transmission has the form (using Eq. (5) to normalize the value of d_o):

$$-u^{-\frac{1}{2}} \ln t = 2\sqrt{\frac{\gamma}{d_o}\bar{k}} \sum_n \left(\frac{f_n g_n}{Q} e^{-n\Delta E/kT}\right)^{\frac{1}{2}} \qquad (10)$$

Given values for ΔE, f_n, and g_n, the value of γ/d_o may be deduced from this expression.

The values for the parameters g_n and f_n for CO_2 and H_2O are presently being evaluated under a separate ARPA funded study. A first estimate of the fine structure effects for CO_2 has been obtained using a more approximate procedure. Here simplified representations for f_n and g_n have been assumed and the value of d_o deduced from the strong line limit calculations carried out previously by Malkmus. The relative intensity factor was assumed to be the same for all line groups (i.e., $f_n = 1$) and the effective line density factor g_n was assumed to have the form $(1 + \epsilon n)^2$. Calculations were carried out for various values of ϵ and ΔE. In order to test the accuracy of this procedure, the low pressure (Doppler lines) emissivity has been evaluated for the 4.3- and 2.7-μ bands of CO_2 (using the curve of growth given in Eq. 6) and compared to the detailed calculations of Malkmus. The results

were found to be relatively insensitive to the value of ΔE as long as it is not too large. Using a value of ΔE equal to hc (667 cm^{-1}), the values for ϵ which gave a "best" representation of the zero pressure calculations were determined by trial. These are shown in Fig. 3. In Figs. 4 to 7 the emissivities are shown for three values of ϵ: 0, ϵ_{best}, and $2\epsilon_{best}$. Reference to these figures shows that a reasonable representation of the Doppler line calculations can be obtained with this formalism throughout the range of optical depths and temperatures for which detailed calculations are available. The corresponding values of d_o^{-1} are shown in Figs. 8 to 12. These are also tabulated at 10 cm^{-1} intervals in Table I.* In Table II the values for the line density are given in the limit $\Delta E \to \infty$ (these values we denote as $1/d_{LR}$). In this case the formalism is equivalent to approximating the total curve of growth at each wavenumber by a single Ladenburg-Reiche function; i.e.,

$$-\ln t = 2\pi \frac{\gamma}{d_{LR}} z\, e^{-z}[J_o(iz)-iJ_1(iz)] \qquad (11)$$

where $z = kud_{LR}/2\pi\gamma$.

In many practical applications the pressures are high enough that Doppler broadening may be ignored. Since, in these cases, the curves of growth for $\Delta E \to 0$ ($\approx 1/S$ distribution) and $\Delta E \to \infty$ (delta function distribution) are quite similar, little accuracy is sacrificed for homogeneous gases by using the simple formalism which obtains in the $\Delta E \to \infty$ limit. This will also be true for inhomogeneous gases so long as the inhomogeneity is not too great. Calculations are currently being carried out to determine the sensitivity of the radiance to the value of ΔE. The results of calcu-

*Tables I and II are given in an Appendix.

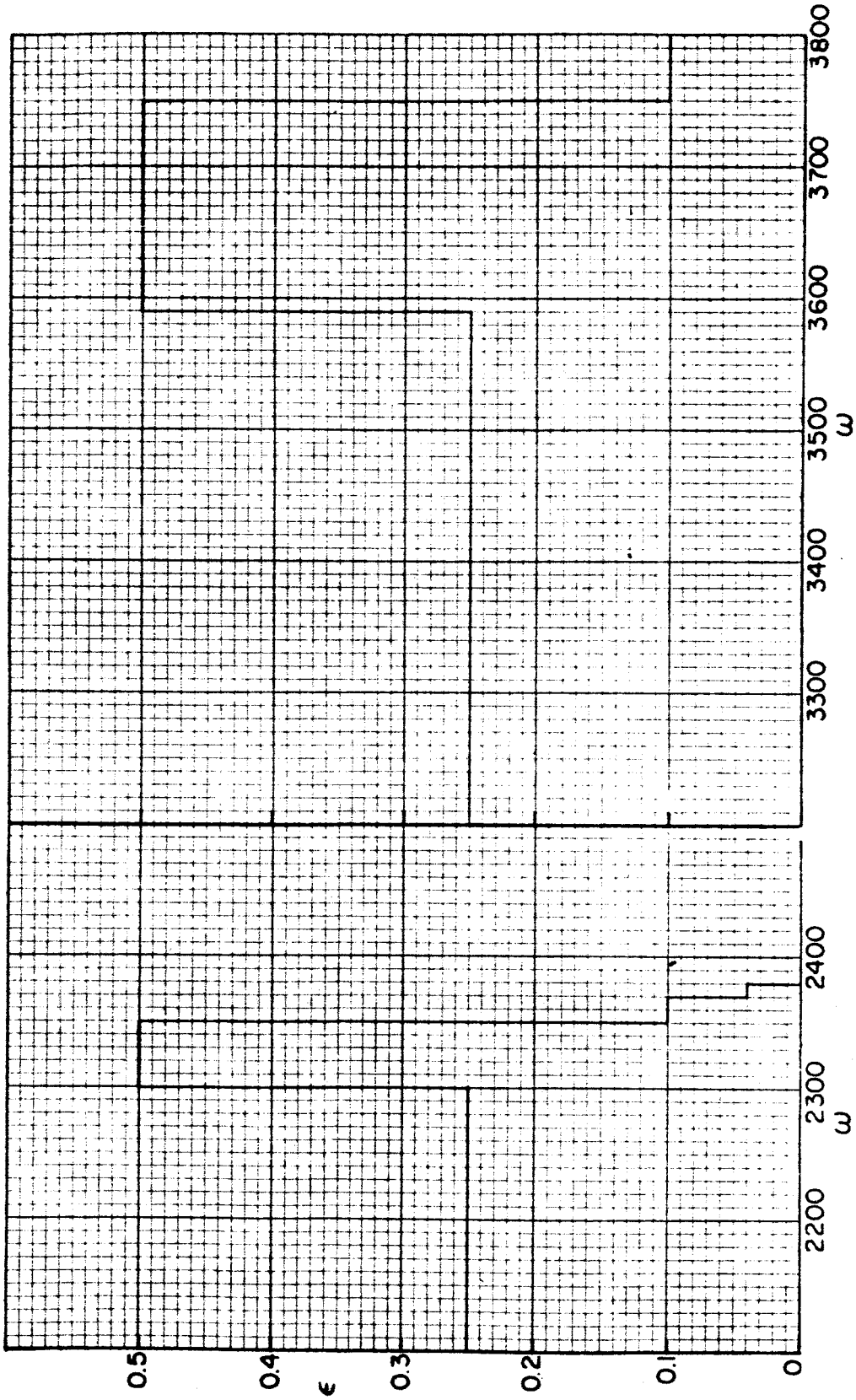

Fig. 3. The line density parameter $\epsilon(\omega)$ for the 2.7- and 4.3-μ bands of CO_2.

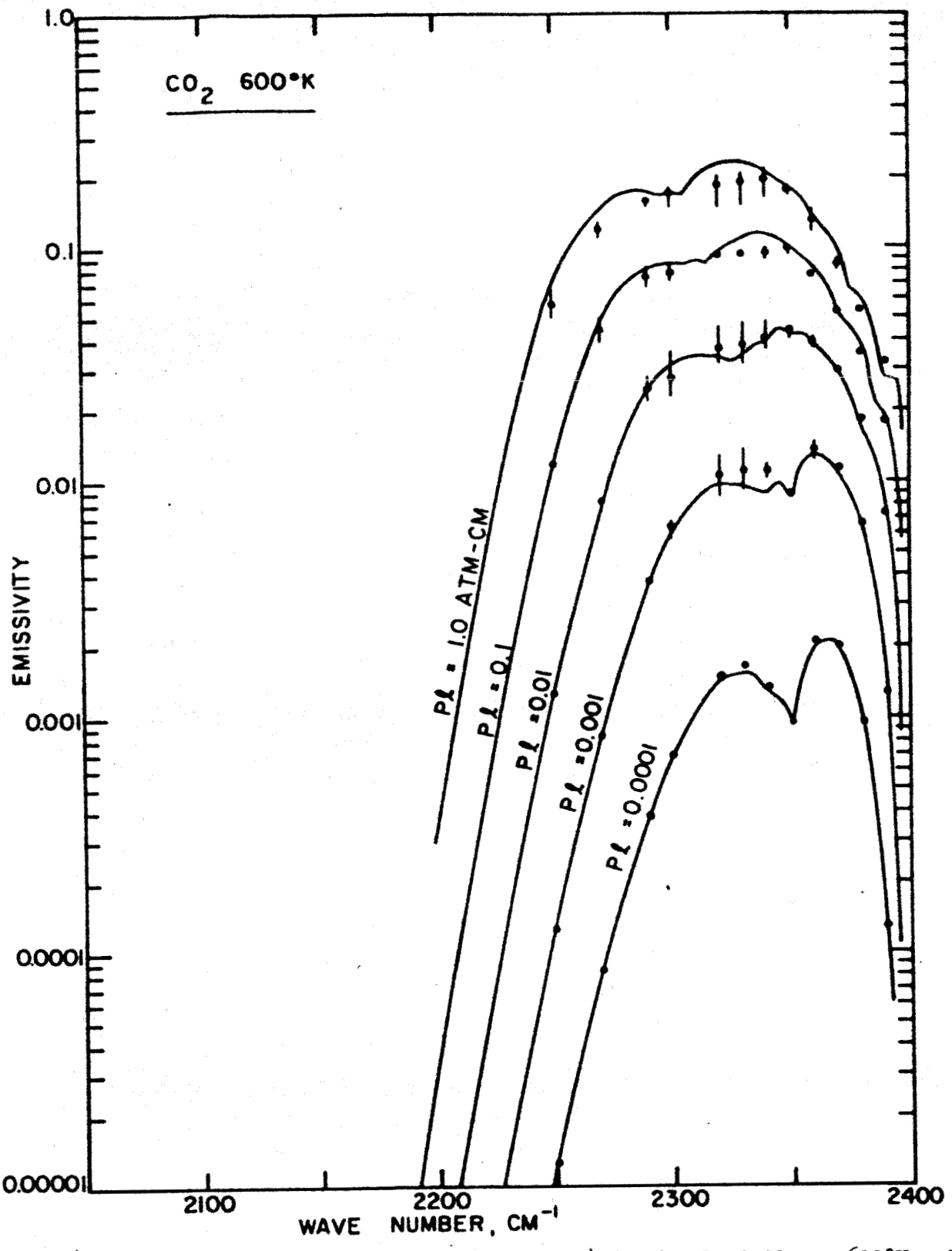

Fig. 4. Comparison of the emissivities in the 4.3-μ band of CO_2 at 600°K and very low pressure (Doppler broadening) calculated using Model 3 radiance with Malkmus' detailed calculations (solid curves). The solid dots correspond to the values of ε given in Table I and the vertical line represents the effect of increasing ε by a factor of 2 or decreasing it to zero. In each case the value of the line spacing parameter d_0 is adjusted so that the collision broadened square root limit agrees with Malkmus' theoretical values.

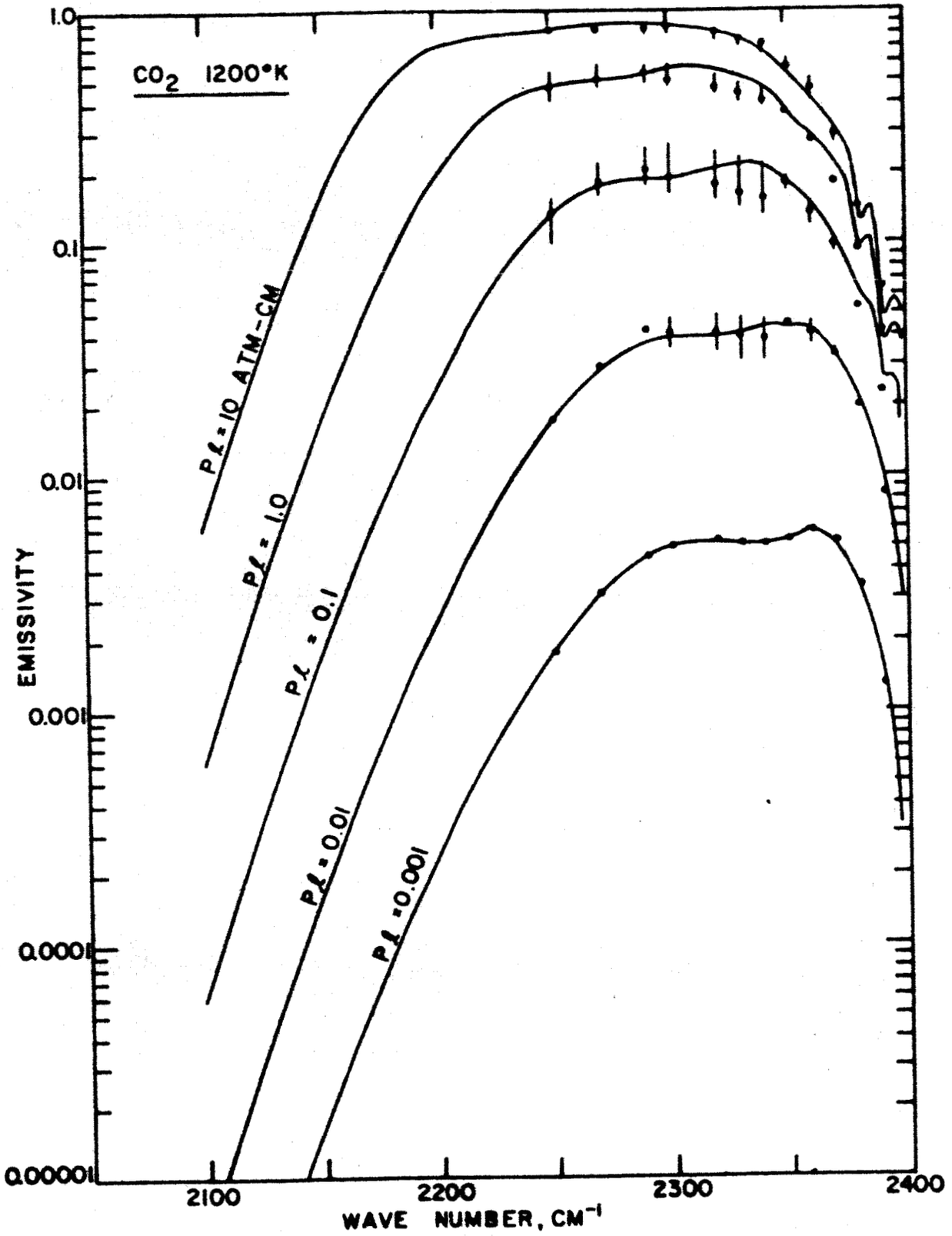

Fig. 5. Comparison of the emissivities in the 4.3-μ band of CO_2 at 1200°K and very low pressure calculated using Model 3 (solid dots) with Malkmus' detailed calculations (solid curves).

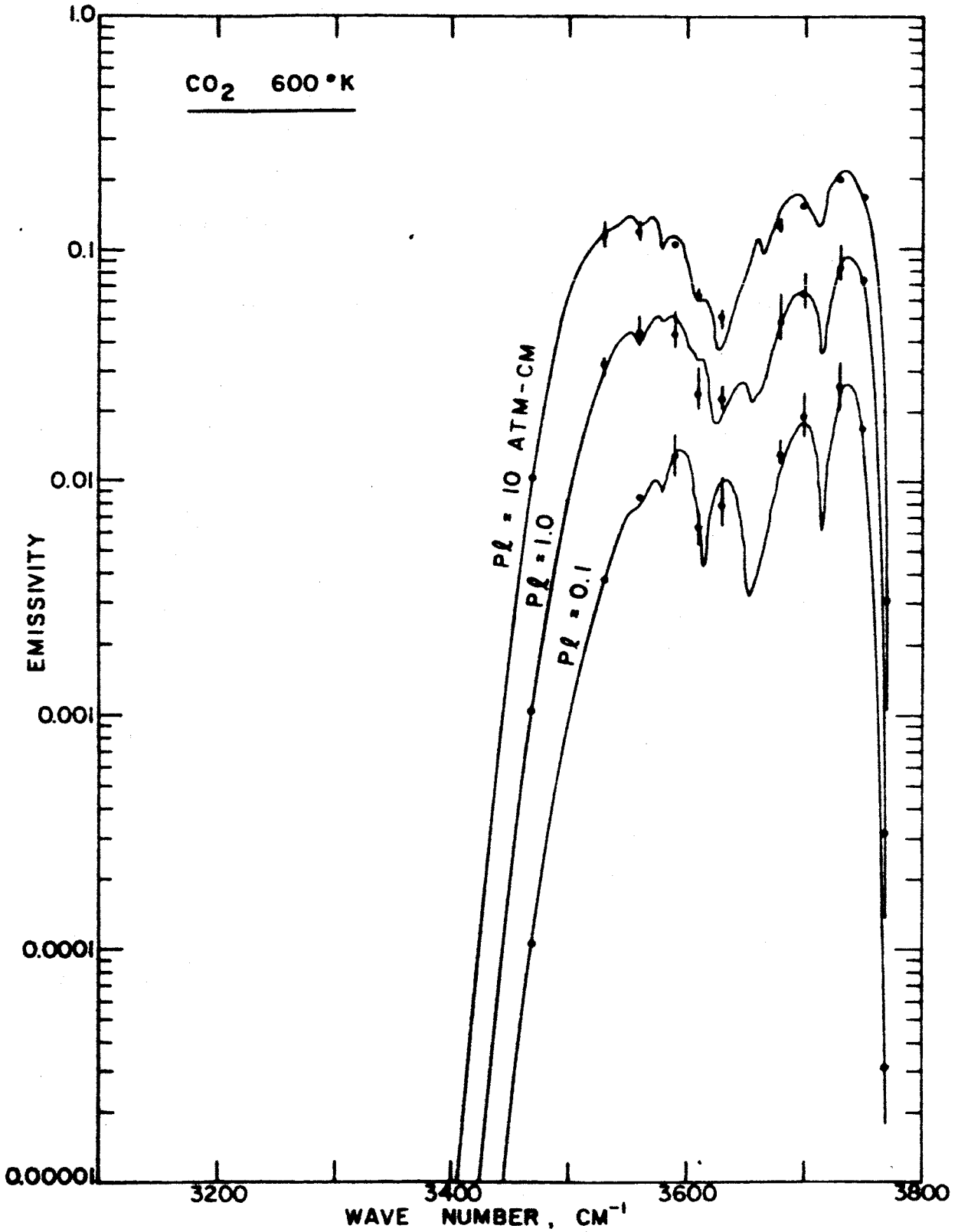

Fig. 6. Comparison of the emissivities in the 2.7-μ band of CO_2 at 600°K and very low pressure calculated using Model 3 (solid dots) with Malkmus' detailed calculations (solid curves).

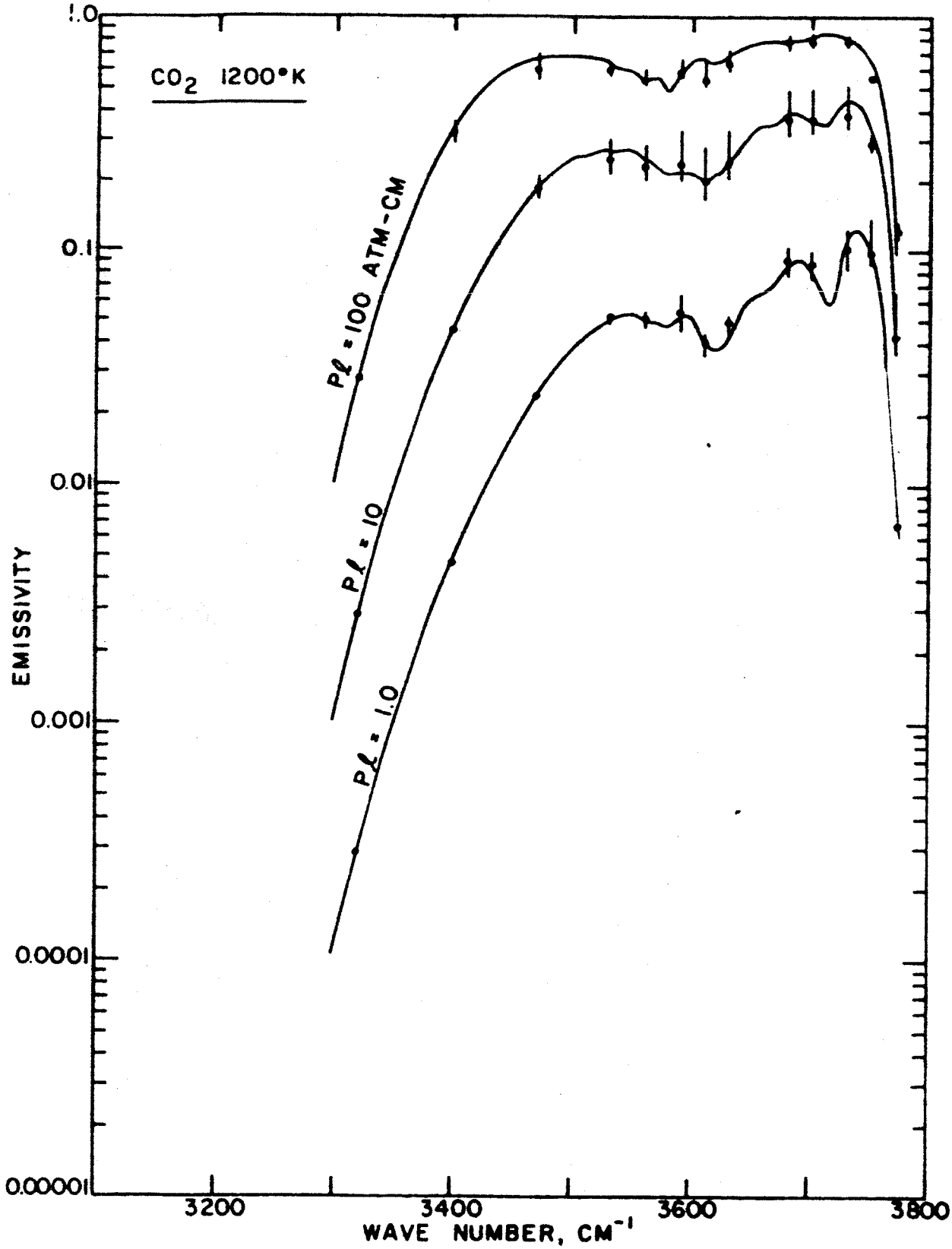

Fig. 7. Comparison of the emissivities in the 2.7-μ band of CO_2 at 1200°K and very low pressure calculated using Model 3 (solid dots) with Malkmus' detailed calculations (solid curves).

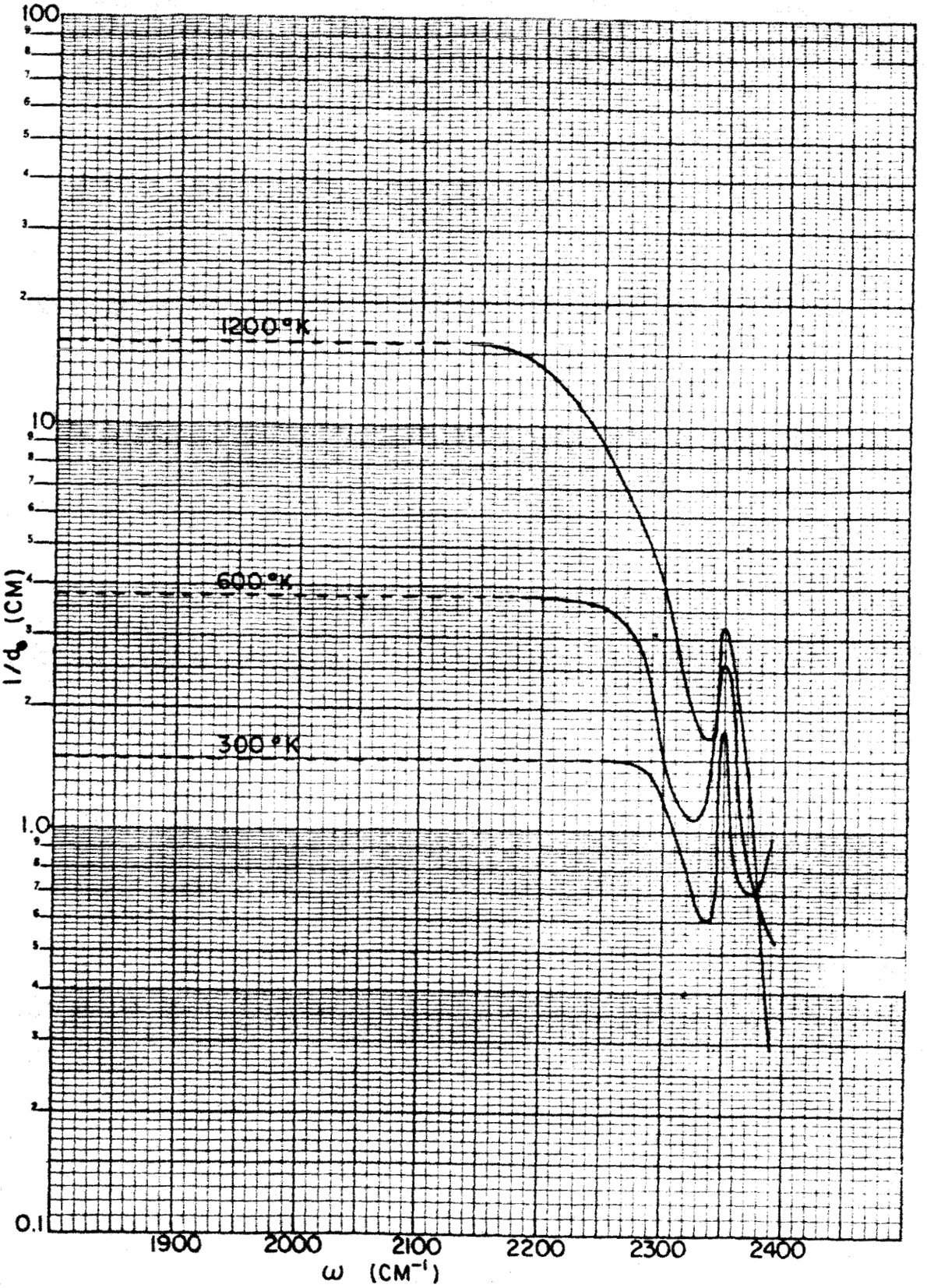

Fig. 8. Values of the line density parameter $1/d_0$ for the 4.3-μ band of CO_2. The dashed portions of the curves are extrapolated values. These data are tabulated in Table I.

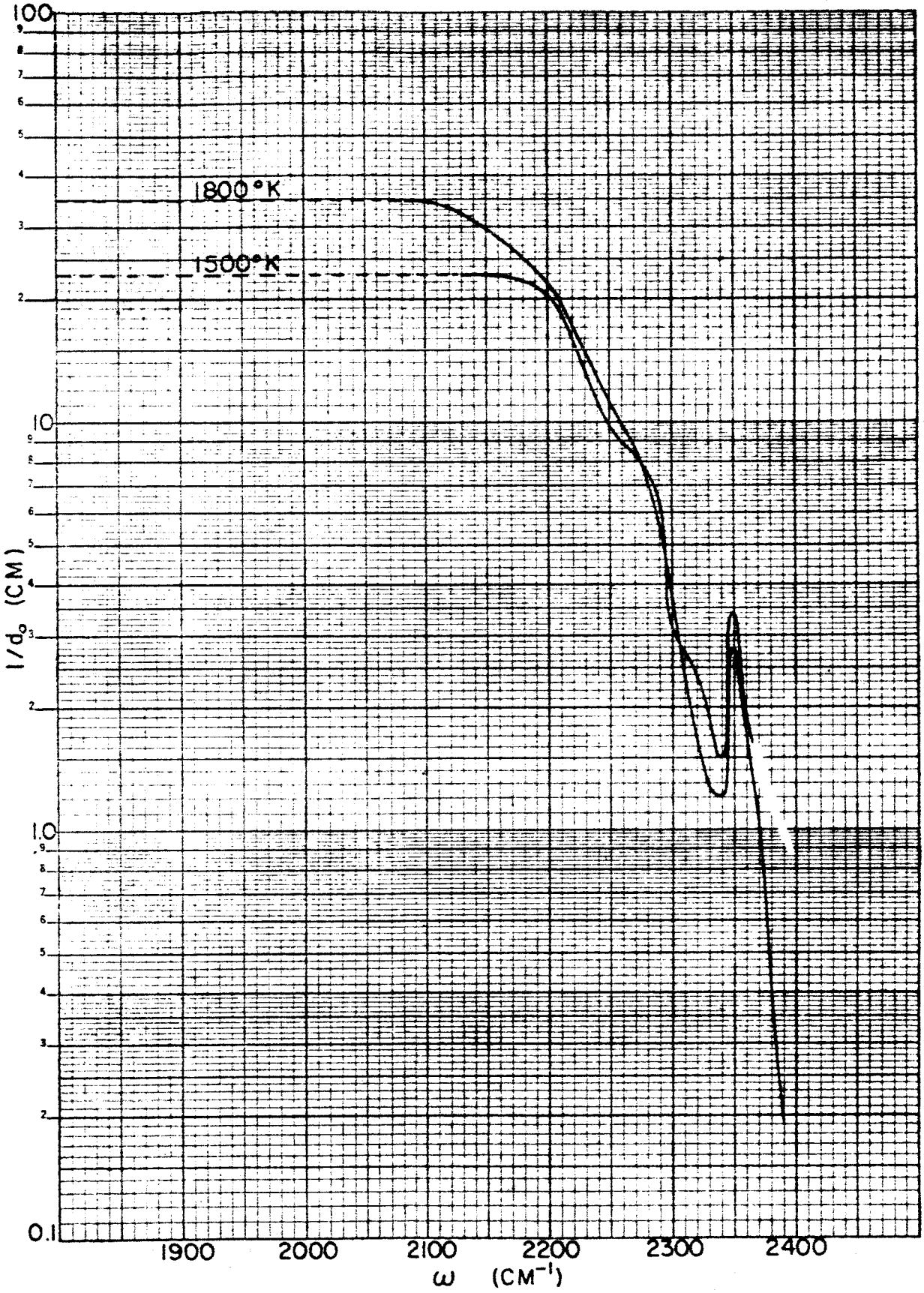

Fig. 9. Values of the line density parameter $1/d_o$ for the 4.3-μ band of CO_2. The dashed portions of the curves are extrapolated values. These data are tabulated in Table I.

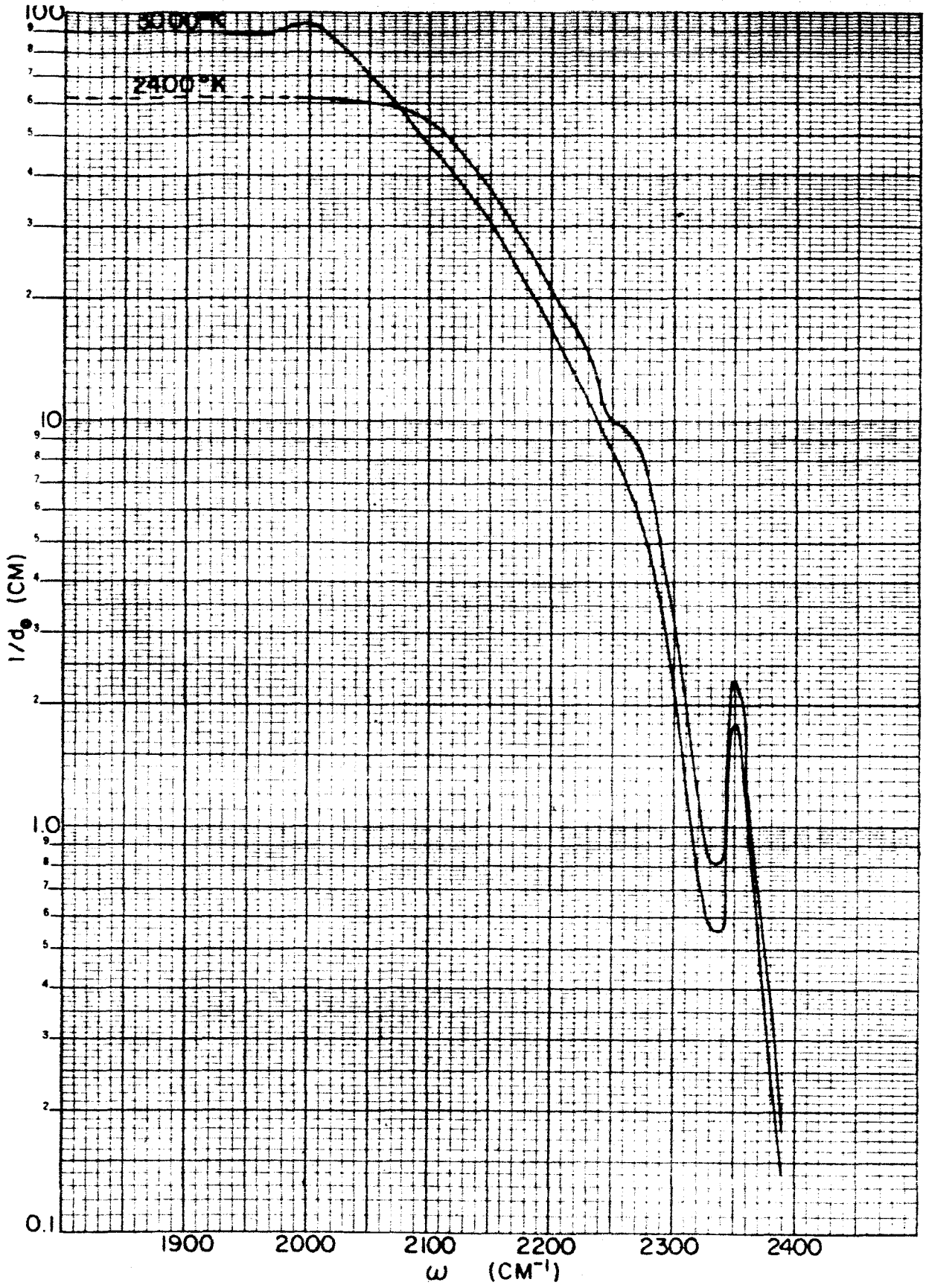

Fig. 10. Values of the line density parameter $1/d_0$ for the 4.3-μ band of CO_2. The dashed portions of the curves are extrapolated values. These data are tabulated in Table I.

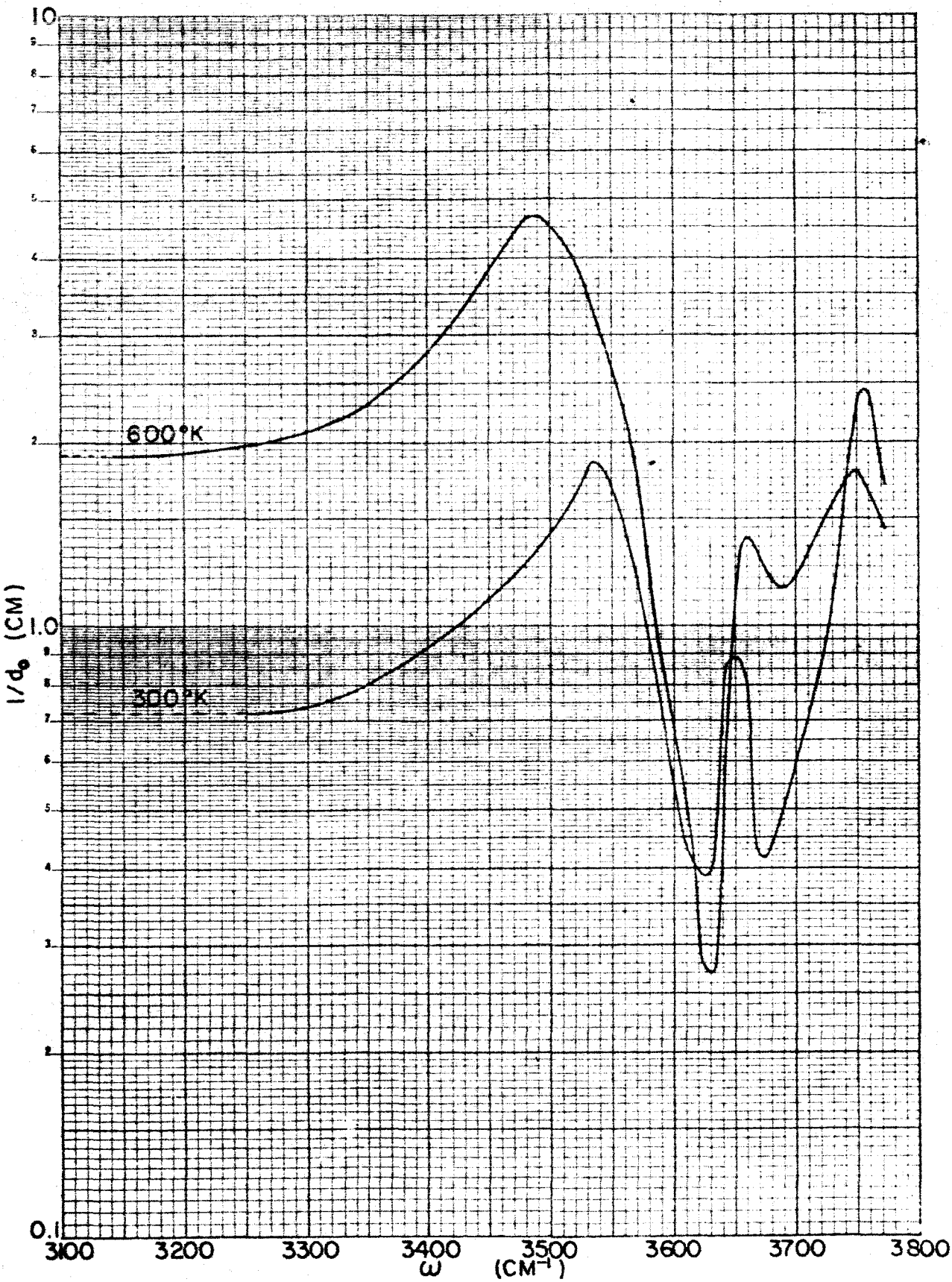

Fig. 11. Values of the line density parameter $1/d_0$ for the 2.7-μ band of CO_2. The dashed portions of the curves are extrapolated values. These data are tabulated in Table I.

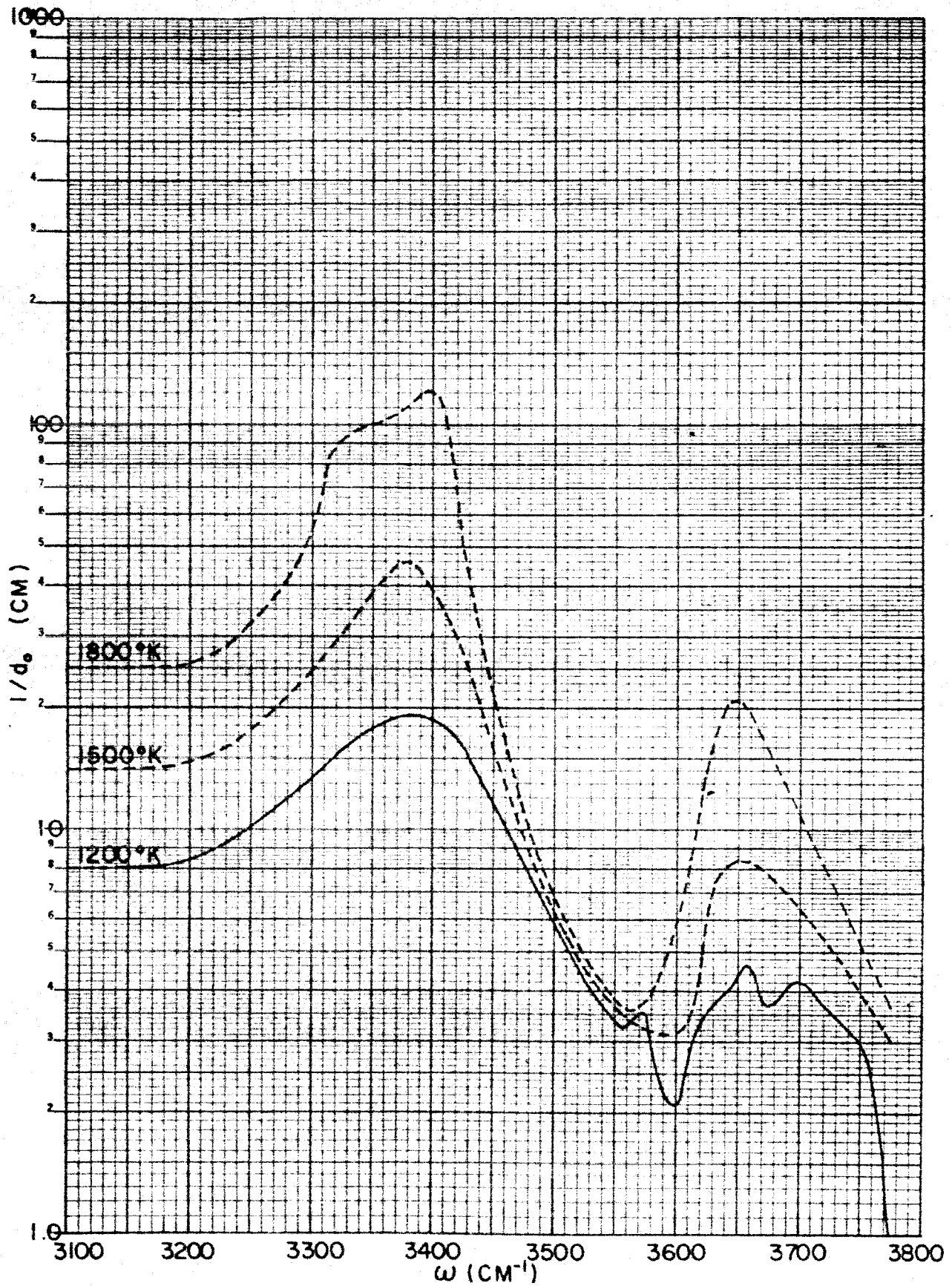

Fig. 12. Values of the line density parameter $1/d_o$ for the 2.7-μ band of CO_2. The dashed portions of the curves are extrapolated values. These data are tabulated in Table I.

lations for a two temperature distribution in which a hot region is viewed through a colder region indicate that the $\Delta E \to \infty$ limit is satisfactory so long as the mass of the cool absorbing gas is not appreciably greater than that of the hot gas. In Figs. 13 and 14 we show the ratio of the radiance calculated in a modified Curtis-Godson approximation for the $\Delta E \to \infty$ limit to the exact value as a function of the ratio of the mass in the hot section to that in the cold section. In this calculation the radiance of the front slab alone was assumed negligible.

In the front slab all the molecules are assumed to be in the ground state ($E_i \gg kT$) and in the rear slab the first N levels are assumed to be equally excited ($E_i/kT_2 \ll 1$; $h_i = 1$ for $i < N$, $h_i = 0$ for $i > N$). In both slabs the total absorption line strength per unit mass of all the excited lines is assumed constant (i.e., $\bar{k}_1 = \bar{k}_2$). It was also assumed that the molecular anharmonicities were sufficiently large that the excited lines do not overlap and that the line widths in the two slabs were equal.

With these assumptions the exact expression for the equivalent width becomes

$$\nu^{-1} W_{exact} = f_{LR}\left(\frac{\bar{k}}{a_1}\left(u_1 + \frac{u_2}{N}\right)\right) - f_{LR}\left(\frac{\bar{k}u_1}{a_1}\right) + (N-1)\, f_{LR}\left(\frac{\bar{k}u_2}{Na_1}\right) \qquad (12)$$

Here u_1 and u_2 are the pathlengths (in mass/unit area) in the front and rear slabs respectively and a_1 is the line width to spacing ratio in the front slab. In the modified Curtis-Godson approximation, the curve of growth of an inhomogeneous gas is replaced by that for a homogeneous gas in which the fine structure parameter $\underline{a}$ is an absorption coefficient

averaged value:

$$\langle a \rangle = \int_0^u a(u)\, k\, du \Big/ \int_0^u \bar{k}\, du \qquad (13)$$

In the present case of equal line widths in the two slabs, the modified Curtis-Godson approximation for the case when the lines are treated individually (equivalent to the $\Delta E \to 0$ limit) yields the exact result.

When the curve of growth of the entire group of lines is approximated by a single Ladenburg-Reiche function (the $\Delta E \to \infty$ limit), the expression for the equivalent width in the Curtis-Godson approximation becomes

$$\gamma^{-1} W_{C.G.} = \frac{u_1 + Nu_2}{u_1 + u_2} f_{LR}\left(\frac{\bar{k}(u_1+u_2)}{\tilde{a}}\right) - f_{LR}\left(\frac{\bar{k}u_1}{a_1}\right) \qquad (14)$$

where $\tilde{a} = \dfrac{u_1 + Nu_2}{u_1 + u_2} a_1$. In Figs. 13 and 14 the ratio $W_{C.G.}/W_{exact}$ is plotted against u_2/u_1 for various values of $\bar{k}u_1/a_1$. Reference to these figures shows that the modified Curtis-Godson approximation gives a good approximation of the equivalent width so long as $u_2/u_1 > 1/3$. At smaller values quite large errors may be incurred.

The accuracy of the approximation does not appear to be too sensitive to the number (N) of hot lines that appear at high temperature so long as N is not too large. However, when the number of hot lines becomes very large, large errors may result. For example, as $N \to \infty$ the ratio $W_{C.G.}/W_{exact}$ becomes

$$1 + \frac{u_1}{u_2}\left[1 - \left(1 + \frac{\bar{k}u_1}{4a_1}\right)^{-\frac{1}{2}}\right] \qquad (15)$$

Here, when the cool front region is optically thick ($\bar{k}u_1/4a_1 \gg 1$) a 50%

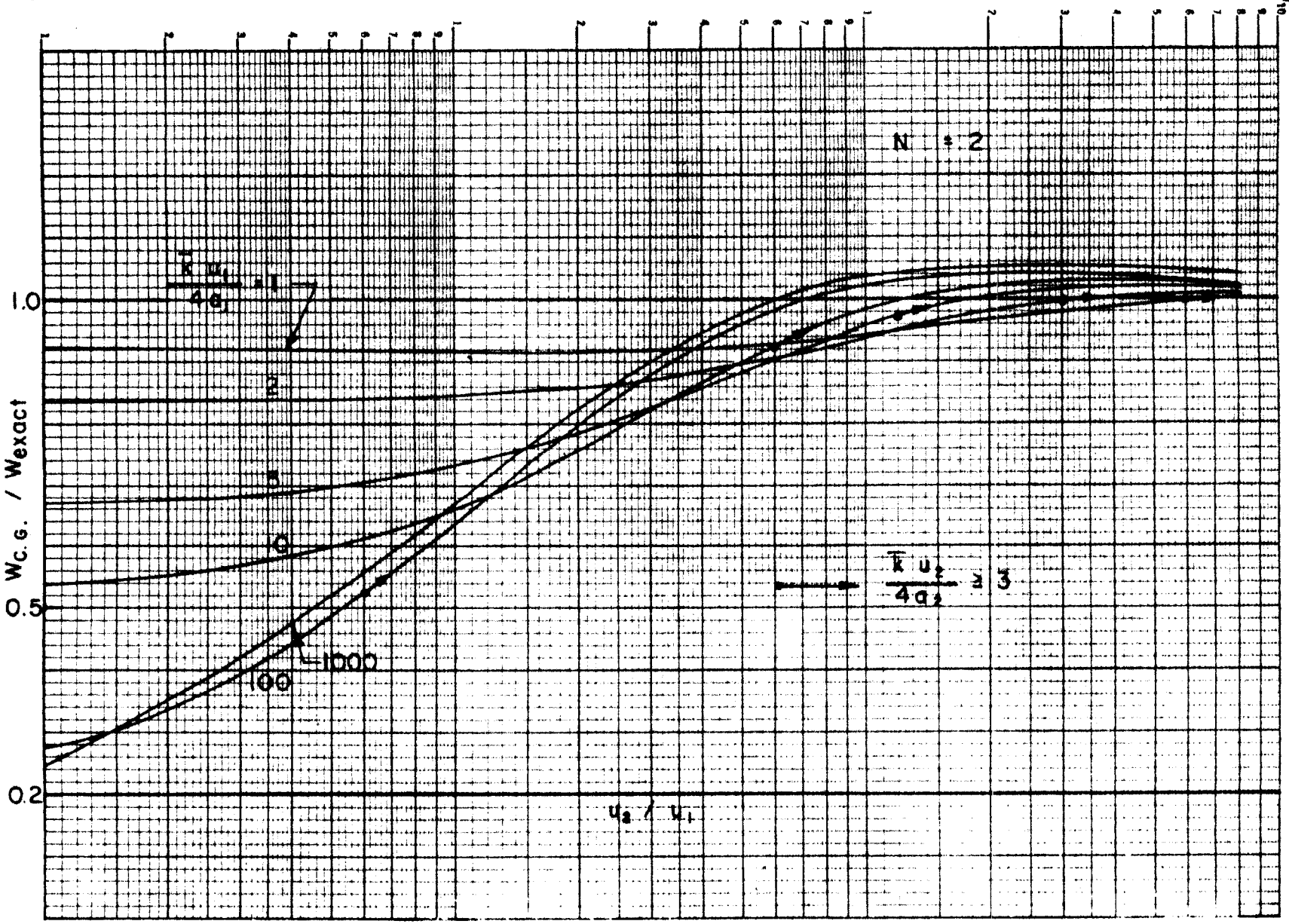

Fig. 13. Effect of hot lines on the emission from high temperature gas viewed through a cool absorbing layer. The ordinate is the ratio of the radiance of a two temperature slab computed in the modified Curtis-Godson approximation to the exact value. The abscissa is the ratio of the mass of the high temperature rear slab to that of the low temperature front slab. In the rear slab two equally intense lines are excited; whereas in the front slab, all the line strength is concentrated in only one of the lines.

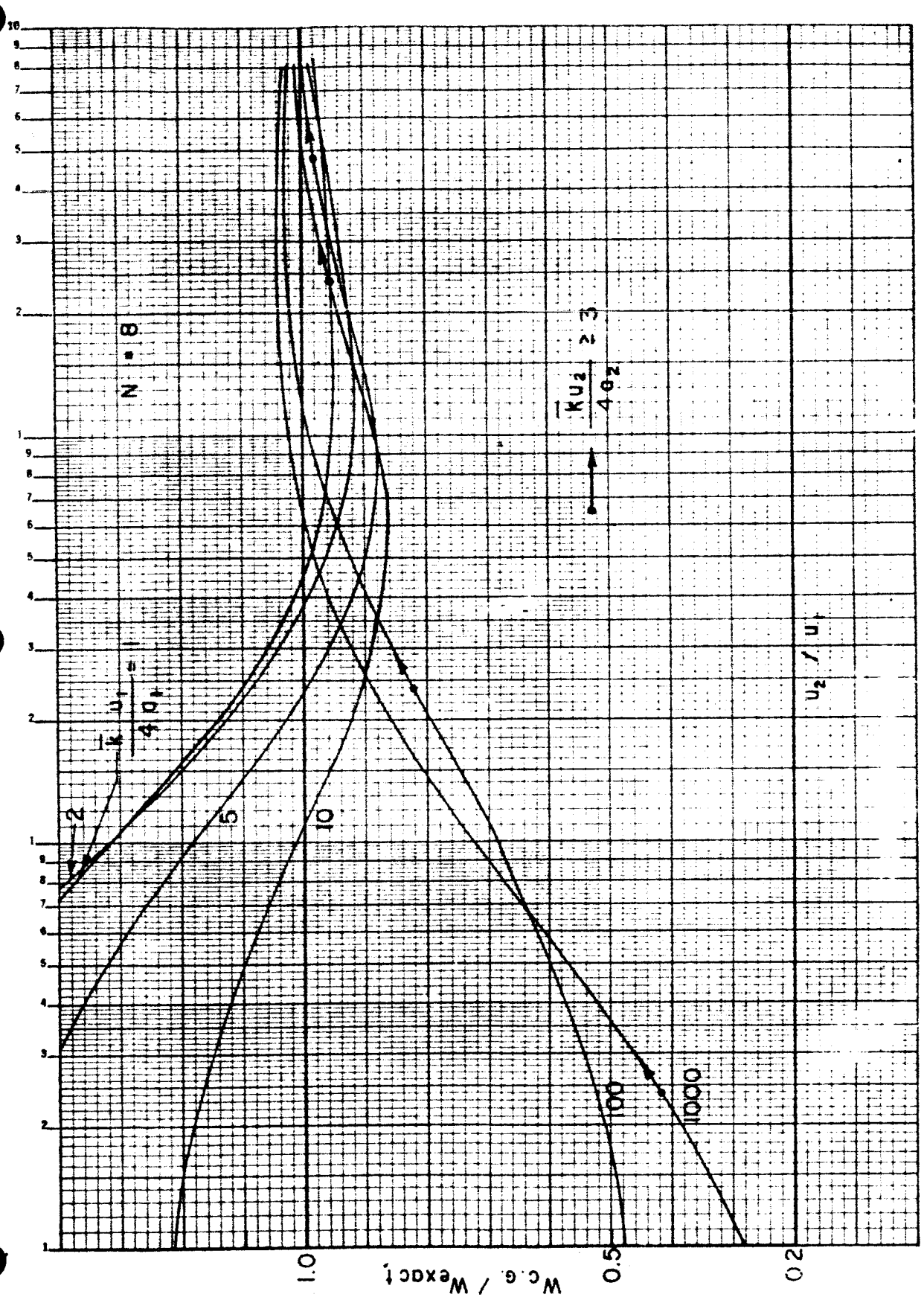

Fig. 14. Effect of hot lines on the emission from a high temperature gas viewed through a cool absorbing layer. This figure is the same as Fig. 13 except the single line in the cool section is divided into eight equally intense lines in the hot section, one of which is the original line.

error is incurred when the hot and cold masses are equal.

Based on these calculations, it appears necessary to ensure that the values of the parameters f_n, g_n, and ΔE are chosen such that the resulting value of the characteristic line spacing d_o of the individual line groups does not vary by much more than a factor of 10 along the portion of the line of sight that includes most of the mass.

III. Determination of the Fine Structure Parameters from Experimental Curves of Growth

The high pressure curves of growth are sufficiently similar for quite different line intensity distributions that it may be difficult to distinguish between different distributions directly from measurements of the transmission versus optical depth unless the data accuracy is exceptionally high. The high pressure curve of growth measurements are expected to yield accurate values for the average absorption coefficient $k(\omega,T)$ and the mean line width to line spacing ratio $\underline{a}(\omega,T)$ $(= \gamma/d)$. To obtain a complete description of the transmission function that will be applicable both to low pressures (where Doppler broadening is important) and to inhomogeneous gases, it is necessary in general also to obtain values for the relative intensity and line density distribution functions, f_n and g_n, for groups of lines which have similar dependencies on temperature. Also required is a reasonable value for the line grouping parameter ΔE. The accuracy with which these must be known depends on the absolute pressures and the degree of inhomogeneity expected. In order to obtain an experimental determination of these quantities, it is necessary to select one or both of two conditions: 1) a homogeneous optically thick path at pressures low enough that Doppler broadening is important; 2) an optically thick inhomogeneous path at intermediate or low pressures.

Doppler broadening will be important when the value of the equivalent width of a characteristic line computed for collision broadening only is less than that based on pure Doppler broadening. Using the approximate expressions in Eqs. (6) and (7) for the corresponding curves of growth, the ratio of these two widths may be expressed in terms of the ratio (r)

of the collision half width to the Doppler half width ($r = \gamma_C/\gamma_D$) and the characteristic opacity of a Doppler broadened line ($\tau_D = Su/\gamma_D$):

$$\frac{W_C}{W_D} = 0.589\ \tau_D \left\{\left(1 + \frac{\tau_D}{4r}\right)\left(\ell n\left[1 + (0.589\ \tau_D)^2\right]\right)\right\}^{-\frac{1}{2}} \qquad (16)$$

This ratio is plotted in Fig. 15. For small values of r, the minimum value of this ratio is roughly $1.7\sqrt{r}$. For water vapor at 2000°K, the value of r at $\omega = 3500\ cm^{-1}$ is about 2P where P is the total pressure (nitrogen broadening). Thus Doppler effects can be important at pressures less than 0.1 atmosphere. Since self-broadening will reduce this critical pressure somewhat, it appears necessary to carry out measurements at pressures of no more than a few hundredths of an atmosphere in order to get an adequate measurement of the curve of growth in the Doppler region.

An alternate method for determining appropriate values of the fine structure parameters f_n, g_n, and ΔE is to carry out measurements of optically thick inhomogeneous paths at moderate pressures. The calculations of the preceding section indicate that the value of radiance of a moderately short hot volume of gas viewed through a longer cooler path may be sensitive to the values of these quantities. In order to get a more quantitative determination of the importance of these parameters, some sensitivity calculations have been initiated. The sensitivity of the radiance to the line grouping parameter ΔE may be seen in Table IIL Here the temperature and concentration profiles shown in Fig. 16 were used as representative distributions. In Table IIIthe ratio of the radiance calculated for various

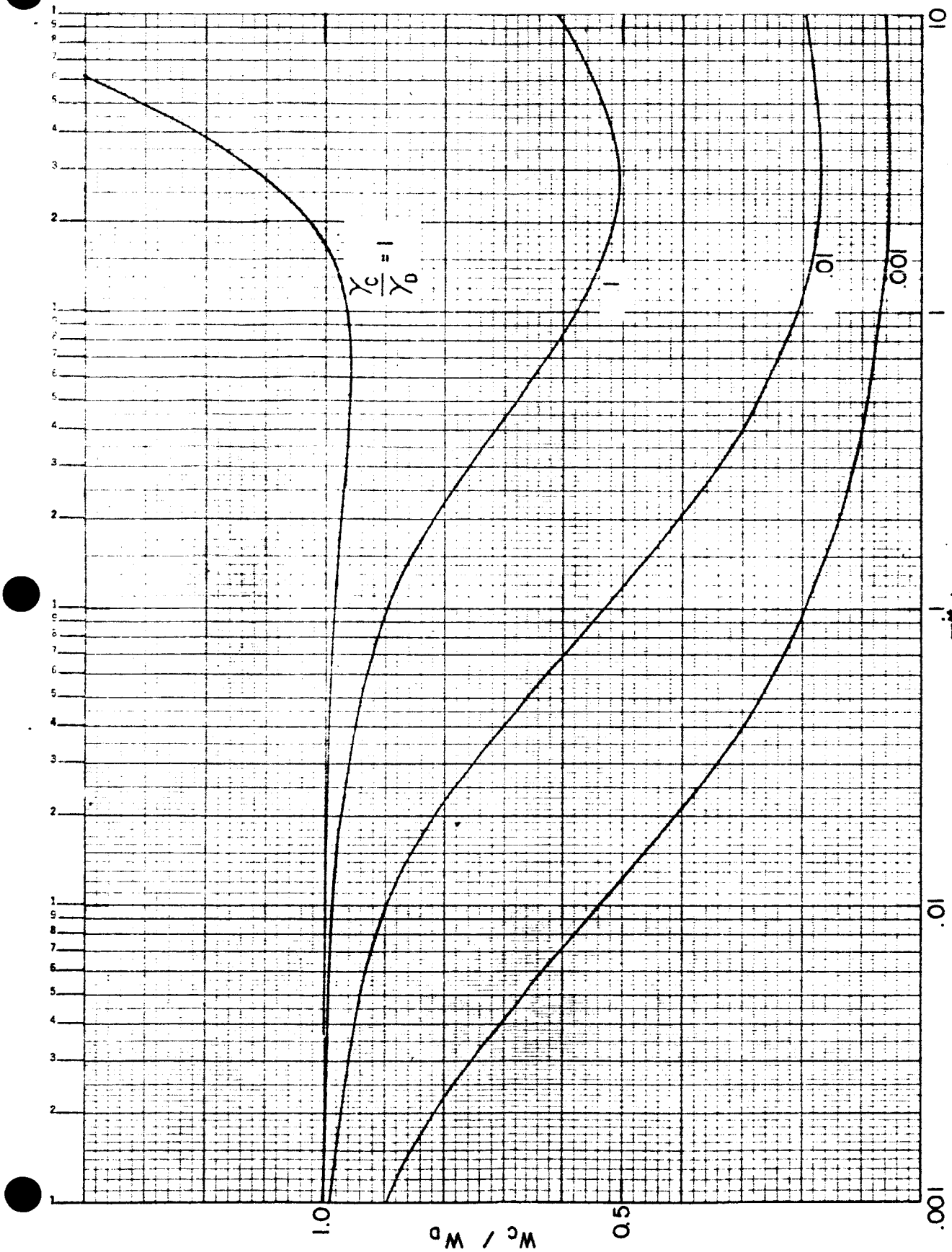

Fig. 15. Ratio of the equivalent width for pure collision broadening (W_C) to that for pure Doppler broadening as a function of the characteristic optical depth for the Doppler line (τ^*/a_D).

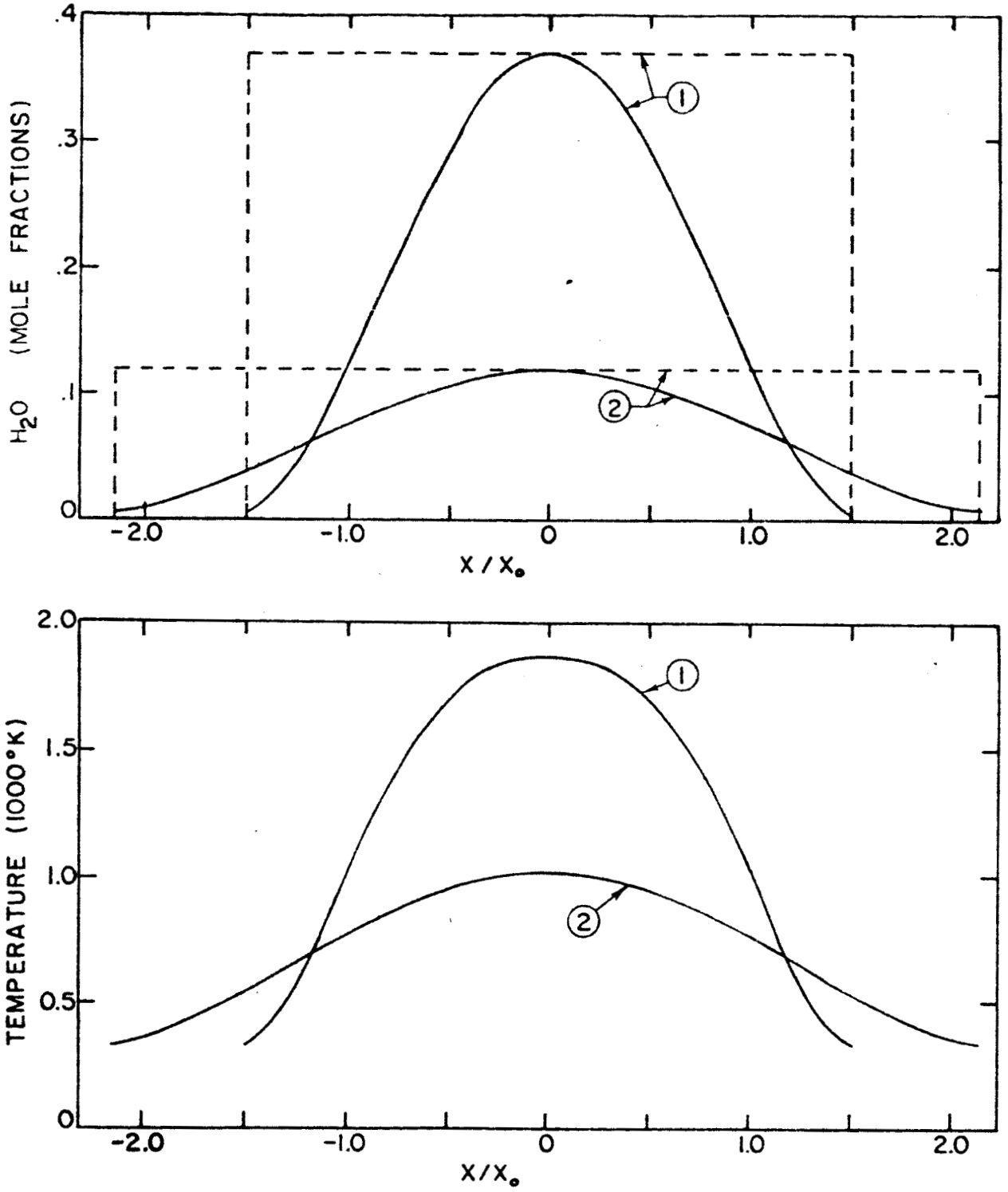

Fig. 16. Temperature and concentration profiles used to test the sensitivity of the radiance calculation to the parameter θ ($= \Delta E/k$). These profiles are typical of profiles found in constant pressure turbulent jets. The values of the computed radiancies for various values of θ at different total pressures, wavenumbers, and characteristic lengths (X_0) are tabulated in Table III. In this Table the profiles labeled "Bell" are the solid curves in the upper figure and those labeled "Uniform" are the dashed curves.

Table III: Sensitivity of the calculated radiance (using Model 3) to the value of the line grouping parameter $\theta = \Delta E/k$ (For Model 3, $\theta = \theta_o \equiv 2300°K$).

ω (cm^{-1})	Pressure (Atm)	T_{max} (°K)	C_{H_2O} (mole fraction)	X_o (meters)	$\alpha(\theta_o)$*	$N_\lambda(\theta_o)$ watts/ster-μ-cm^2	$\frac{N_\lambda(\theta_o/2)}{N_\lambda(\theta_o)}$	$\frac{N_\lambda(\infty)}{N_\lambda(\theta_o)}$
3950	.0109	1865	Bell	10	.081	.259	1.20	.74
				100	.192	.57	1.21	.58
		1013		10	.047	.0080	1.23	.75
				100	.114	.0185	1.20	.70
		1865	Uniform	10	.099	.211	1.22	.63
				100	.249	.46	1.21	.50
		1013		10	.054	.0066	1.26	.72
				100	.140	.0155	1.21	.68
3950	.109	1865	Bell	3	.229	.61	1.15	.79
				30	.582	1.41	1.11	.78
		1013		3	.168	.0246	1.16	.87
				30	.454	.062	1.12	.86
		1865	Uniform	3	.346	.46	1.16	.69
				30	.757	.84	1.07	.72
		1013		3	.218	.020	1.17	.83
				30	.554	.046	1.11	.83
3950	1.09	1865	Bell	1	.659	1.77	1.07	.90
				10	.981	1.32	0.89	1.02
		1013		1	.569	.086	1.10	.94
				10	.946	.082	.94	.97
		1865	Uniform	1	.853	.85	1.04	.83
				10	.999	.147	.69	1.15
		1013		1	.689	.057	1.05	.90
				10	.981	.031	.86	.98
1800	.0109	1865	Bell	10	.064	.031	1.21	.68
				100	.166	.076	1.20	.65
		1013		10	.039	.0038	1.21	.77
				100	.110	.0102	1.18	.79
		1865	Uniform	10	.094	.026	1.23	.55
				100	.255	.061	1.22	.55
		1013		10	.053	.0032	1.22	.72
				100	.154	.0084	1.20	.74

*Absorptivity for $\theta = \theta_o$

values of θ ($= \Delta E/k$) to that for $\theta = 2300°K$ are tabulated at two wavelengths for various conditions. Except for θ the values of the various spectroscopic quantities are those corresponding to our Model 3 for water vapor. The results of these calculations indicate that the radiance of an optically thick inhomogeneous gas, in which the outer region is cooler than the interior, is moderately sensitive to the value of θ. The effects are most pronounced at low pressures where Doppler broadening is important or for very thick gases for which the absorptivity is close to unity.

These sensitivity analyses are continuing and will be applied also to determining the importance of the parameters f_n and g_n.

Once an appropriate form for the curve of growth has been selected (i.e., when values have been assigned to the parameters θ, g_n, and f_n) the fine structure parameter γ/d_o may be evaluated by fitting this curve of growth to the experimental data. In Part I of this progress report, the results of our application of this procedure to the measurements of water vapor made by a number of investigators were described. In that analysis the procedure was equivalent to fitting a Ladenburg-Reiche curve of growth, using the approximation given in Eq. 5. Oppenheim also fits his measured curves of growth for the 2.7-μ water band at 1200°K with a Ladenburg-Reiche curve (see Fig. 4 of Part I). As Malkmus has pointed out previously (see also Part I, pp. 49-53) the extrapolation of moderately optically thick data to the square root region with a Ladenburg-Reiche curve always results in an underestimate of the square root limit and thus of the value of $1/d_{LR}$. The errors depend on the optical thicknesses of the original data and are usually small enough that they may be ignored in a first approximation. For practical purposes we have found that the

most convenient approach is to use Ladenburg-Reiche fits for the initial determinations of the line density parameters and then refine the description of the fine structure by recomputing the actual emissivity or absorptivities that were actually measured, using more reasonable curves of growth and adjusting the fine structure parameters to get an improved fit. This approach is necessitated when the published data give detailed results for the inferred Ladenburg-Reiche parameters but only representative results of the original absorptivity measurements.

In Fig. 17 we show the Ladenburg-Reiche parameters $1/d_{LR}$ (from Fig. 3 of Part I) deduced from various measurements. The dashed line in this figure (Model 2), which is a fit to the experimental points, was used to recompute a number of the original experimental data. These comparisons are given in Part I of this progress report. The present Model 3 curve of growth, which gives a better description of the weak lines, has been used to compute the absorptivities of water vapor in the 2.7-μ region measured by Simmons. Improved values for the fine structure parameter d_o^{-1} were evaluated on the basis of these comparisons. These are tabulated in Table VII (in Section V-1) and comprise the present Model 3 values. A representative comparison with Simmon's data is shown in Fig. 18.

In order to compare with the previous Ladenburg-Reiche fits, a Ladenburg-Reiche curve has been fitted to Model 3 in the square root limit (this is the simplified Model 3a). In Fig. 17 the resulting Ladenburg-Reiche parameters $(1/d_{LR})$ are compared to the values deduced in the initial fits. As expected the new values are somewhat higher on the average, although the experimental scatter does not make the differences too significant. In Fig. 19 a similar comparison with Oppenheim's fine

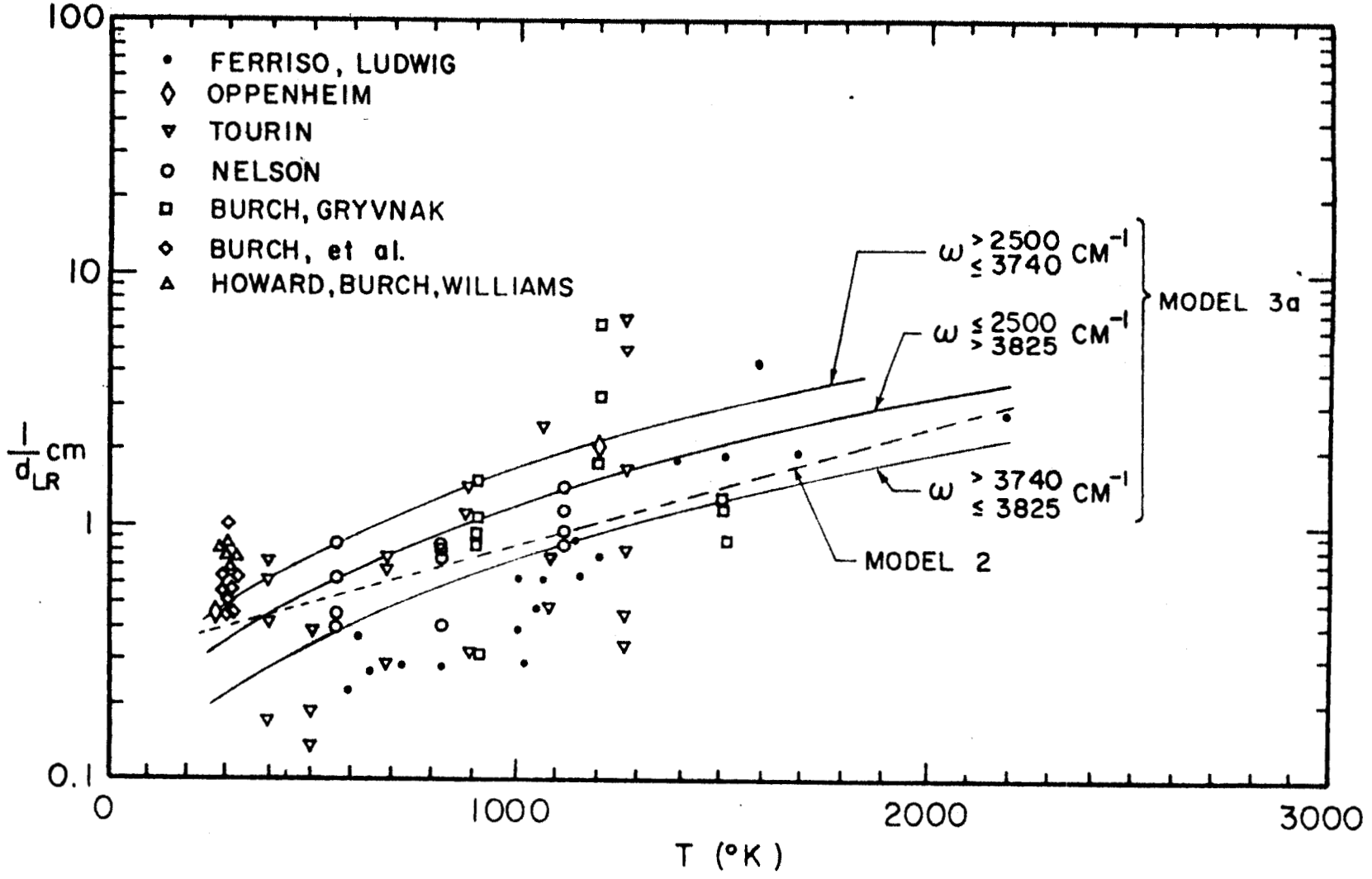

Fig. 17. Comparison of Model 3a line densities for water vapor with various measured values.

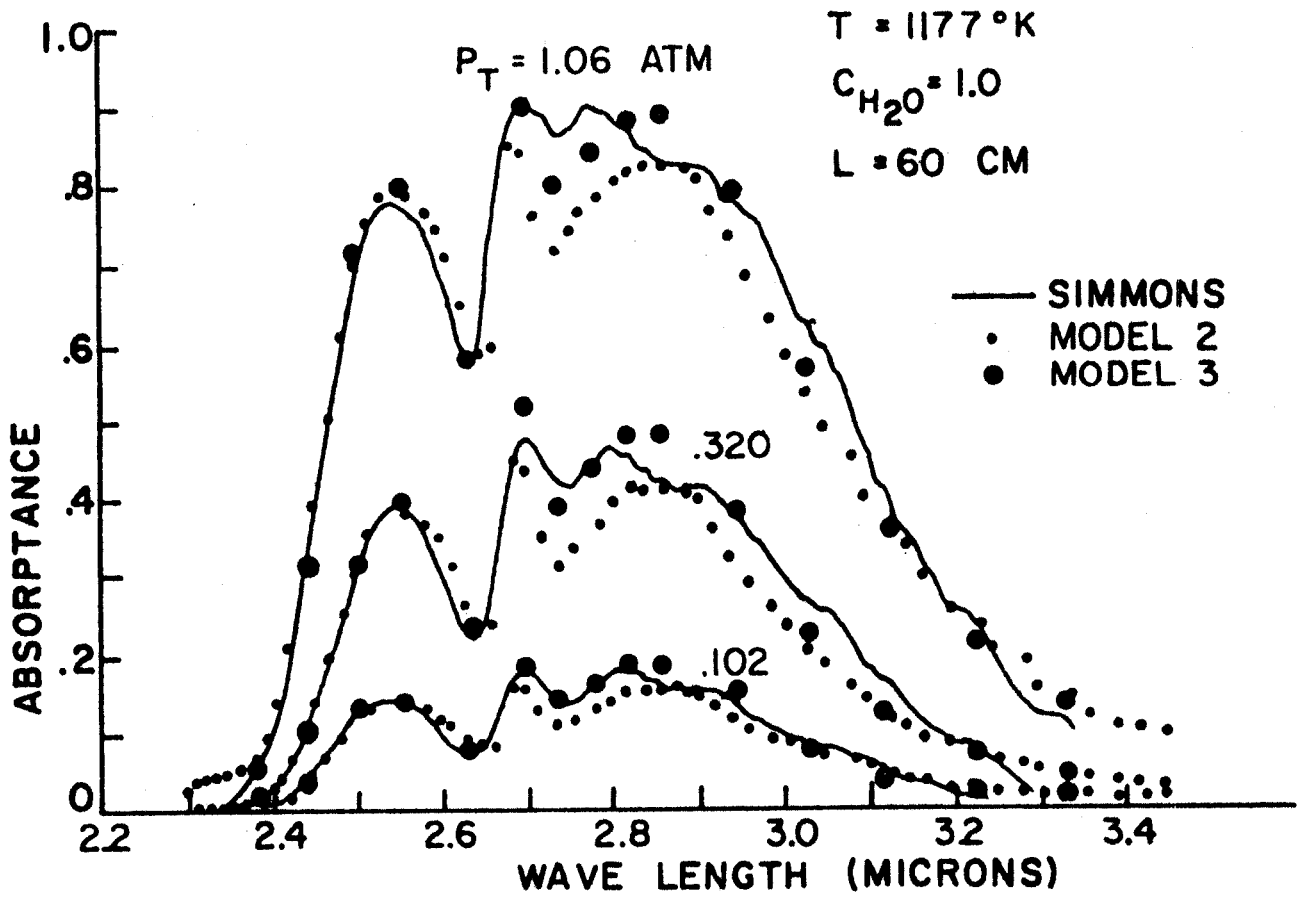

Fig. 18. Comparison of Model 3 with Simmon's measurements of the 2.7-μ band of water vapor.

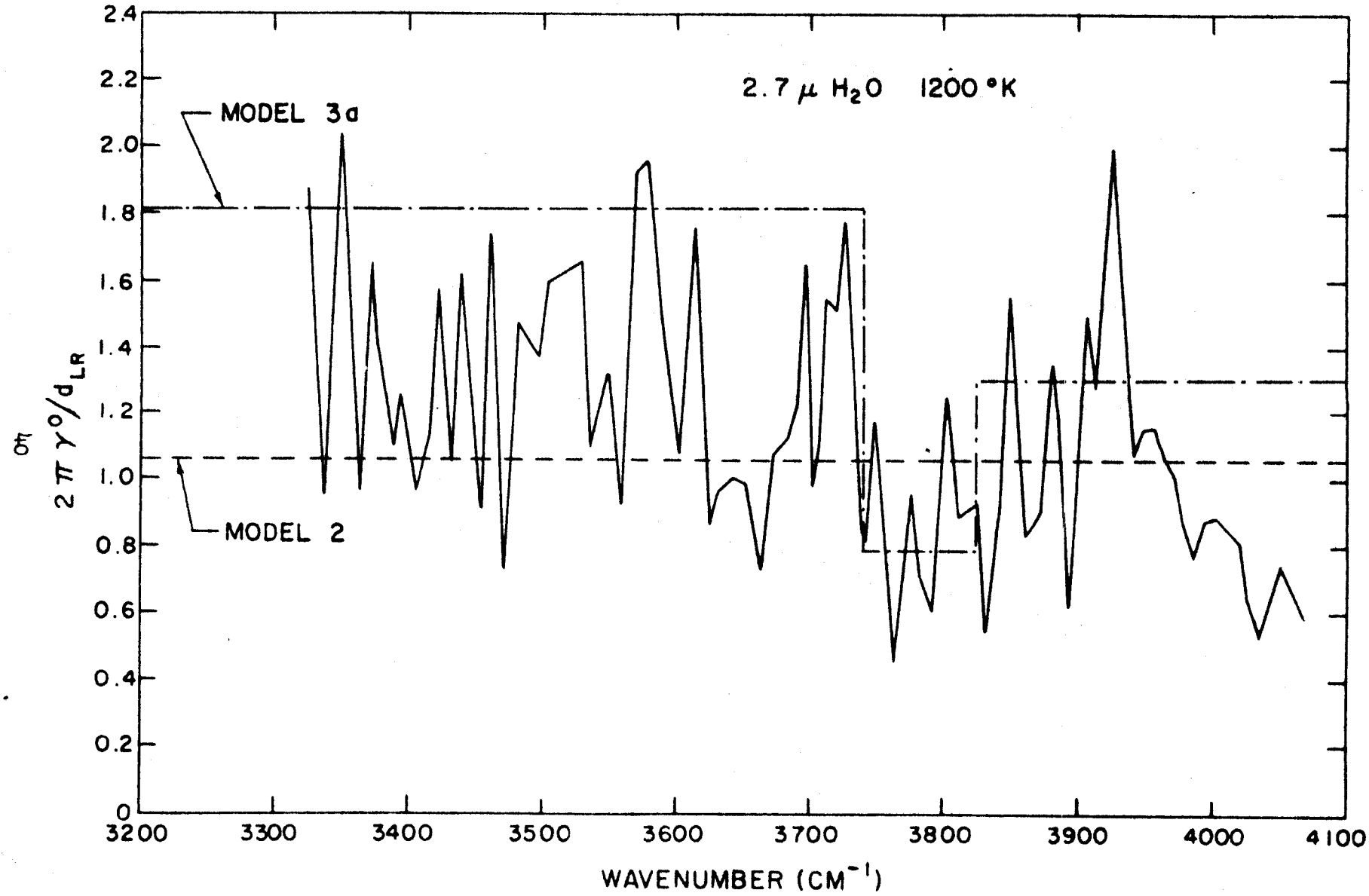

Fig. 19. Comparison of Model 2 and Model 3a with the Ladenburg-Reiche parameters measured by Oppenheim for the 2.7-μ band of water vapor.

structure parameter $2\pi\gamma^{o}/d_{LR}$ at 1200°K is shown. Again the Model 3a values are appreciably higher than the Ladenburg-Reiche fit values.

These comparisons indicate that direct Ladenburg-Reiche extrapolations of the present experimental data to the square root limit may underestimate the curve of growth in this region. At present it is felt that Model 3 or Model 3a provide the most reliable methods for extrapolating to thick paths although more detailed measurements of the fine structure at thick paths and as a function of wavenumber are required.

IV. Line Widths

1) Collision Widths for H_2O

For molecules having an appreciable dipole moment but small moments of inertia, it is appropriate to allow for two contributions to the self-broadened line width: a resonant term ($J_1 = J_2 \pm 1$), and a non-resonant term. For optical collision diameters which are independent of the collision energy, we would expect a temperature dependence (at constant pressure) of $T^{-\frac{1}{2}}$ for the non-resonant term and T^{-1} for the resonant term. Calculations by Benedict and Kaplan for H_2O-H_2O collisions near room temperature indicate that the actual variation of individual line widths with temperature can deviate considerably from these simple representations. Also, the variation from one line to another can be quite large (more than a factor of 2). Even if detailed line by line calculations of both line strengths and collision widths were available throughout the temperature range of interest, the problem of incorporating these results into a formalism simple enough to be used for practical calculations from inhomogeneous gases is formidable. For the present purposes, the most practical approach appears to be to use a very simple two or three parameter representation which is based on a simple physical model (constant optical collision diameter) and determine the values of the fit parameters either from detailed theoretical calculations carried out for representative conditions or from measurements of the fine structure parameters. At the present time, most of the available experimental data for individual line widths is limited to temperatures near 300°K. Benedict and Kaplan have carried out theoretical calculations for H_2O-N_2 collisions for a number of water vapor lines for temperatures up to 2400°K.

The present sensitivity analyses for the fine structure terms indicate that, so long as the analytical formalism is tied to experiment or precise theory in certain limiting regions (such as the square root limit), quite crude (but physically reasonable) representations of the fine structure terms can give reasonably accurate representations of the spectra except under rather unique experimental conditions.

The long path high temperature measurements to be carried out in the near future together with the continuing sensitivity analyses will be used to give better values to the appropriate fine structure parameters and to check and refine the formal representation of the fine structure. The sensitivity analyses are considered very important in the determination of the reliability and accuracy of the formalism for application to conditions not attainable in the laboratory.

For water vapor the approximation of optical collision diameters which vary as a power of the temperature leads to an expression for the line width of the form

$$\gamma_C = \sum_j (\gamma_j)_{STP} P_j \left(\frac{273}{T}\right)^{n_j} + (\gamma^*_{H_2O})_{STP} P_{H_2O} \left(\frac{273}{T}\right)^{n^*}$$

Here P_j is the partial pressure of the jth broadener and $(\gamma_j)_{STP}$ is the line width at STP due to collision with this species (including the non-resonant self broadening collisions). $\gamma^*_{H_2O}$ is the contribution of resonant collisions. For the present model, the available data do not warrant a sophisticated representation. Thus, for Model 3 we use the constant collision diameter temperature exponents $n_j = 0.5$ and $n^* = 1.0$.†

† The calculations of Benedict and Kaplan indicate that a somewhat improved representation for H_2O-N_2 collisions can be obtained with $n_j = 0.6$-0.7 instead of 0.5.

In Table IV we have listed values for the half widths of H_2O for both self and foreign-gas broadening taken from various sources. Also listed is a set of recommended values based on these data.

2) Collision Line Widths for CO_2 and CO

For a mixture of gases, we express the collision line width of CO_2 and CO in the form

$$\gamma = \sum_{i=1}^{N} (\gamma_i)_{STP} P_i \left(\frac{273}{T}\right)^{n_i} \qquad (17)$$

where P_i is the pressure in atmospheres of the ith species, $(\gamma_i)_{STP}$ is the line width at STP due to collisions with that species and n_i an exponent describing the temperature dependence of the line width. Both CO_2 and CO have a relatively large number of rotational energy levels excited even at room temperature because of their high moments of inertia. Thus the contributions to the line width due to resonant collisions ($J_1 = J_2 \pm 1$) are relatively small. As a first approximation, therefore, we may take $n_i = \frac{1}{2}$ for all species i. In Table V we have listed values for the half widths for CO_2 and CO for both self and foreign-gas broadening taken from various sources. Also, in Table V we indicate a set of recommended values based on these data.

3) Doppler Line Widths

The line half width at half height due to Doppler broadening alone may be expressed in the form

$$b_D = \omega_o \sqrt{(2 \ln 2)kT/mc^2}$$

where ω_o is the wavenumber at the line center and m the molecular weight.

Table IV: Collision broadened line half widths at half height for H_2O at STP (in cm^{-1})*

Broadener	H_2O	N_2	O_2	CO_2	Ar	He	Source
	5.2a	a					Burch, et al.
	0.54	.087		.12	.065		Vasilevsky and Neporent
	0.53	.092	.044				Benedict and Kaplan
Model 3	0.53	0.09	0.04	0.12			

*Values for foreign gas broadeners have been scaled to 273°K according to $\gamma \sim T^{-\frac{1}{2}}$. For self broadening, $\gamma \sim T^{-1}$ was used.

Table Va: Collision broadened line half widths at half height for CO_2 at STP (in cm^{-1})*

Broadener	CO_2	N_2	O_2	H_2	A	He	Source
	0.1						Madden
	< 0.12						Adel
	0.079						Benedict, Silvermann
	0.088						Kostkowski
		.067					Kaplan, Eggers
		.12					Adel
		.06					Kostkowski
	1.3a	a	.81a	1.17a	.78a	.59a	Burch, et al.
Model 3	.09	0.07	.055	.08	.05	.04	

Table Vb: Collision broadened line half widths at half height for CO at STP (in cm^{-1})*

Broadener	CO	N_2	O_2	H_2	A	He	Source
	1.02a	a		.85a	.78a	.64a	Burch, et al.
		a	.87a	1.25a		.72a	Cross and Daniels
	.042			.043	.022	.019	Penner and Weber
				.067	.064	.027	Matheson
	.057						Benedict, et al. ($m \approx 15$)
Model 3	.05	.05	.04	.05			

*These data have been scaled to 273°K according to $\gamma \sim T^{-\frac{1}{2}}$ at constant pressure.

V-1. Summary of Current Radiance Calculation (Model 3)*

1) Radiance Calculation

The spectral radiance is evaluated from

$$\frac{dI_\nu}{d\Omega} = - \int B_\nu^o(T) \frac{d}{ds} \left(\exp\left[- \sum_i \tau_{\nu,i} \right] \right) ds \quad . \tag{18}$$

The optical depth $\tau_{\nu,i}$ for the ith species is evaluated from a sum over line groups:

$$\tau_{\nu,i} = \sum_{n=0}^{\infty} (\tau_{\nu,i})_n \quad . \tag{19}$$

The optical depth of the nth group is evaluated from the curve of growth $[f(\tau^*, a_C, a_D)]$ using the modified Curtis-Godson approximation:

$$(\tau_{\nu,i})_n = f(\tau_n^*, \bar{a}_{C,n}, \bar{a}_{D,n}) \tag{20}$$

where τ_n^* is the optical depth in the just overlapping line approximation:

$$\tau_n^* = \int_o^s k_n \, ds \ , \tag{21}$$

and $\bar{a}_{C,n}$ and $\bar{a}_{D,n}$ are mean values for the fine structure parameters:

$$\bar{a}_{C,n} = \frac{1}{\tau_n^*} \int_o^s \frac{\gamma_C}{d_n} k_n \, ds \ , \tag{22}$$

*The work described in this section was developed principally under Contract No. AF19(628)-4360.

$$\bar{a}_{D,n} = \frac{1}{\tau_n^*} \int_0^s \frac{\gamma_D}{d_n} k_n \, ds \quad . \tag{23}$$

Here γ_C and γ_D are values for the collision broadened and Doppler broadened half-widths, respectively. The absorption coefficient for the nth group is evaluated from

$$k_n = \bar{k}(T) \, f_n \, e^{-n\theta/T} \Big/ \left[\sum_{n=0}^{\infty} f_n \, e^{-n\theta/T} \right] \quad , \tag{24}$$

and the line density $1/d_n$ from

$$\frac{1}{d_n} = g_n / d_o(T) \quad . \tag{25}$$

The mean absorption coefficient $\bar{k}$ and the line spacing parameter d_o are tabulated functions of temperature and frequency. The coefficients g_n and f_n are temperature independent and are tabulated versus n for each frequency. The parameter θ can be a function of frequency but usually is assigned a unique value. (When θ is put equal to infinity, a simpler formalism results. This is summarized in Section V-2).

2) Curves of Growth: $\left(f(\tau^*, \bar{a}_C, \bar{a}_D)\right)$

The curve of growth for combined collision and Doppler broadening is evaluated from the expression

$$f(\tau^*, \bar{a}_C, \bar{a}_D) = \sqrt{1 - y^{-\frac{1}{2}}} \, \tau^* \tag{26}$$

where

$$y = \left[1 - \left(\frac{\tau_C}{\tau^*} \right)^2 \right]^{-2} + \left[1 - \left(\frac{\tau_D}{\tau^*} \right)^2 \right]^{-2} - 1 \quad , \tag{27}$$

and where the pure collision curve of growth is approximated by

$$\tau_C = \tau^*\left(1 + \tau^*/4\bar{a}_C\right)^{-\frac{1}{2}} , \tag{28}$$

and the pure Doppler curve of growth by

$$\tau_D = 1.7\ \bar{a}_D \left[\ell n\left[1+(0.589\ \tau^*/\bar{a}_D)^2\right]\right]^{\frac{1}{2}} . \tag{29}$$

For τ_C much different from τ_D, f is approximately equal to the larger of τ_C or τ_D.

3) Mean Absorption Coefficients $[\bar{k}(T)]$

i) H_2O: Tabulated in Table II of Reference 1.

ii) CO_2: Tabulated in Table IV of Reference 1.

iii) CO: Tabulated in Table III of Reference 1.

iv) Carbon: Tabulated in Table VIII of present report. (Appendix)

4) Collision Line Half Widths

The line shape due to collisions with like or unlike molecules is approximated by a Lorentz line shape. The line half width at half height of the ith molecule is assumed to be the same for all lines and to be given by the form

$$\gamma_{C_i} = \sum_j \left[\left(\gamma_{ij}\right)_{STP} p_j \left(\frac{273}{T}\right)^{n_{ij}}\right] + \left(\gamma^*_{ii}\right)_{STP} p_i \left(\frac{273}{T}\right)^{n^*_{ii}} \tag{30}$$

Here p is the partial pressure in atmospheres of the jth species and the sum is to be carried out over all species. The values of $\left(\gamma_{ij}\right)_{STP}$, n_{ij}, $\left(\gamma^*_{ii}\right)_{STP}$, and n^* are given in Table VI.

Table VI: Model Values for the Collision Line Width Parameters (Model 3)*

Molecule (i)	Broadener (j)	$(\gamma_{ij})_{STP}$	n_{ij}	$(\gamma^*_{ii})_{STP}$	n^*_{ii}
H_2O	H_2O	(0.09)	0.5	0.14	1.0
	N_2	0.09	0.5	0	
	O_2	0.04	0.5	0	
	H_2	(0.05)	0.5	0	
	CO_2	0.12	0.5	0	
	CO	(0.10)	0.5	0	
CO_2	CO_2	0.09	0.5	0	
	H_2O	(.07)	0.5	0	
	N_2	0.07	0.5	0	
	O_2	0.06	0.5	0	
	H_2	.08	0.5	0	
	CO	(.06)	0.5	0	
CO	CO	0.05	0.5	0	
	H_2O	(.05)	0.5	0	
	CO_2	(.05)	0.5	0	
	H_2	0.05	0.5	0	
	N_2	0.05	0.5	0	
	O_2	.04	0.5	0	

*Except for the values in parentheses, these values are based on experimental or theoretical data. Because of the fairly large differences between some of the measurements, these data should be considered preliminary. No experimental data were found for the broadeners for which values given are in parentheses. The values shown are strictly guesses.

5) Doppler Half-Widths

The half-width (γ_D) at half-height of Doppler broadened lines is given by the expression

$$\gamma_D = (5.94 \times 10^{-6}) \frac{\omega}{M^{\frac{1}{2}}} \left(\frac{T}{273}\right)^{\frac{1}{2}} \qquad (31)$$

where ω is the wavenumber and M the molecular weight (in gms/mole).

6) Fine Structure Parameters

Table VIIa. Values for the parameters $1/d_o$, f_n, g_n, and θ.

Molecule	$1/d_o(T,\omega)$	g_n	f_n	θ (°K)	Remarks
H_2O	$\frac{1}{d_o(273°K)} \left[T/273\right]^{\frac{1}{2}}$ (tabulated in Table VIIb below)	1.0	1.0	2300	
CO_2	Tabulated in Table I (Appendix)	$(1+\epsilon n)^2$	1.0	960	$\epsilon(\omega)$ is tabulated in Table I
CO	0.29 cm (constant value)	1.0	n+1	3123	

Table VIIb. Line Density for H_2O at 273°K

$\frac{1}{d_o(273°K)}$ (cm)	Wavenumber (cm^{-1})
.33	$\omega \leq 2500$
.46	$2500 < \omega \leq 3740$
.20	$3740 < \omega \leq 3825$
.33	$\omega > 3825$

V-2. Summary of Simplified Radiance Calculation (Model 3a)

1) Radiance Calculation

This simplified formalism results when all the lines for each species are grouped together. It may be obtained as the limit $\theta \to \infty$. Thus the optical depth for the ith species is given by

$$\tau_{\nu,i} = f(\tau^*, \bar{a}_C, \bar{a}_D) \tag{32}$$

where

$$\tau^* = \int_0^s \bar{k}(T)\, ds$$

$$a_C = \frac{1}{\tau^*} \int \frac{\gamma_C}{d_{LR}} \bar{k}\, ds$$

$$a_D = \frac{1}{\tau^*} \int \frac{\gamma_D}{d_{LR}} \bar{k}\, ds$$

2) Curve of Growth $\left(f(\tau^*, a_C, a_D)\right)$

Same as for Model 3.

3) Mean Absorption Coefficient $[\bar{k}(T)]$

Same as for Model 3.

4) Collision Line Width

Same as for Model 3.

5) Doppler Line Widths

Same as for Model 3.

6) Fine Structure Parameter ($1/d_{LR}$)

The values of $1/d_{LR}(T)$ may be obtained from the tabulated values of $1/d_o(T)$ (Model 3) according to

$$\frac{1}{d_{LR}} = \frac{1}{d_o} \frac{\left[\sum_{n=0}^{\infty} f_n^{\frac{1}{2}} g_n^{\frac{1}{2}} e^{-n\theta/2T}\right]^2}{\left[\sum_{n=0}^{\infty} f_n e^{-n\theta/T}\right]} \tag{33}$$

where θ is the value used in Model 3.

i) H_2O:

Since, for Model 3, $f_n = g_n = 1$, Eq. (33) becomes

$$\frac{1}{d_{LR}} = \frac{1}{d_o} \left(\frac{1+e^{-\theta/2T}}{1-e^{-\theta/2T}}\right)$$

This is plotted in Fig. 17 but is not tabulated.

ii) CO_2:

$1/d_{LR}$ tabulated in Table II. (Appendix)

iii) CO:

$1/d_{LR}$ from Eq. (33): not tabulated.

APPENDIX

Table I

FINE STRUCTURE PARAMETERS FOR CO_2 (THETA = 960.)

4.3 MICRON BAND

1/DD (CM.)

1/CM	MICRON	300 K	600 K	1200 K	1500 K	1800 K	2400 K	3000 K	EPSLON
2000	5.00	1.50	3.80	16.00	23.00	35.00	62.00	94.00	.25
2010	4.97	1.50	3.80	16.00	23.00	35.00	61.80	92.00	.25
2020	4.95	1.50	3.80	16.00	23.00	35.00	61.50	87.00	.25
2030	4.92	1.50	3.80	16.00	23.00	35.00	61.00	82.00	.25
2040	4.90	1.50	3.80	16.00	23.00	35.00	60.70	77.00	.25
2050	4.87	1.50	3.80	16.00	23.00	35.00	60.50	72.00	.25
2060	4.85	1.50	3.80	16.00	23.00	35.00	59.70	67.00	.25
2070	4.83	1.50	3.80	16.00	23.00	35.00	59.00	61.00	.25
2080	4.80	1.50	3.80	16.00	23.00	35.00	58.00	57.00	.25
2090	4.78	1.50	3.80	16.00	23.00	35.00	56.40	52.00	.25
2100	4.76	1.50	3.80	16.00	23.00	34.50	55.00	48.00	.25
2110	4.73	1.50	3.80	16.00	23.00	34.20	51.50	44.00	.25
2120	4.71	1.50	3.80	16.00	23.00	33.50	48.50	41.00	.25
2130	4.69	1.50	3.80	16.00	23.00	32.50	45.00	37.50	.25
2140	4.67	1.50	3.80	16.00	23.00	31.20	41.00	34.00	.25
2150	4.65	1.50	3.80	16.00	23.00	30.00	37.50	31.00	.25
2160	4.62	1.50	3.80	15.70	22.60	28.30	34.80	27.50	.25
2170	4.60	1.50	3.80	15.30	22.50	26.80	30.50	24.50	.25
2180	4.58	1.50	3.80	15.00	22.20	25.30	27.00	21.60	.25
2190	4.56	1.50	3.80	14.60	21.50	23.80	24.00	19.20	.25
2200	4.54	1.50	3.80	14.00	20.30	22.00	21.00	17.00	.25
2210	4.52	1.50	3.75	13.20	18.70	20.00	18.80	14.80	.25
2220	4.50	1.50	3.73	12.30	16.00	17.30	17.00	13.00	.25
2230	4.48	1.50	3.70	11.30	13.50	15.00	14.90	11.20	.25
2240	4.46	1.50	3.65	10.10	11.30	13.00	12.10	9.80	.25
2250	4.44	1.50	3.60	9.10	10.00	11.20	10.00	8.50	.25
2260	4.42	1.50	3.48	8.00	9.00	10.00	9.60	7.40	.25
2270	4.40	1.50	3.25	7.00	8.40	8.90	9.00	6.20	.25

Table I (Con't)

FINE STRUCTURE PARAMETERS FOR CO2 (THETA = 960.)
4.3 MICRON BAND
1/DO (CM.)

1/CM	MICRON	300 K	600 K	1200 K	1500 K	1800 K	2400 K	3000 K	EPSLON
2280	4.38	1.45	2.90	6.00	7.70	7.40	7.30	4.90	.25
2290	4.36	1.40	2.35	5.10	6.70	5.80	5.10	3.50	.25
2300	4.34	1.20	1.50	4.10	3.20	4.20	3.20	2.20	.50
2310	4.32	1.00	1.25	3.15	2.75	2.50	2.10	1.30	.50
2320	4.31	.80	1.10	2.25	2.40	1.70	1.20	.80	.50
2330	4.29	.63	1.10	1.80	1.90	1.30	.83	.57	.50
2340	4.27	.61	1.40	1.70	1.50	1.20	.85	.56	.50
2350	4.25	1.80	2.60	3.20	3.40	2.80	2.30	1.80	.10
2360	4.23	.83	1.50	2.20	2.00	1.70	1.50	1.10	.10
2370	4.21	.71	.86	1.30	1.50	1.10	.70	.50	.04
2380	4.20	.73	.67	.67	.57	.44	.39	.25	.00
2390	4.18	.97	.56	.29	.23	.20	.19	.14	.00

Table I (Con't)

FINE STRUCTURE PARAMETERS FOR CO2 (THETA = 960.)
2.7 MICRON BAND
1/DD (CM.)

1/CM	MICRON	300 K	600 K	1200 K	1500 K	1800 K	2400 K	3000 K	EPSLON
3080	3.24	.72	1.90	8.00	14.00	25.00			.25
3090	3.23	.72	1.90	8.00	14.00	25.00			.25
3100	3.22	.72	1.90	8.00	14.00	25.00			.25
3110	3.21	.72	1.90	8.00	14.00	25.00			.25
3120	3.20	.72	1.90	8.00	14.00	25.00			.25
3130	3.19	.72	1.90	8.00	14.00	25.00			.25
3140	3.18	.72	1.90	8.00	14.00	25.00			.25
3150	3.17	.72	1.90	8.00	14.00	25.00			.25
3160	3.16	.72	1.91	8.10	14.00	25.00			.25
3170	3.15	.72	1.91	8.15	14.10	25.00			.25
3180	3.14	.72	1.92	8.20	14.20	25.00			.25
3190	3.13	.72	1.92	8.30	14.50	25.20			.25
3200	3.12	.72	1.93	8.50	14.70	25.80			.25
3210	3.11	.72	1.93	8.70	15.00	26.40			.25
3220	3.10	.72	1.94	8.90	15.30	27.20			.25
3230	3.09	.72	1.95	9.30	15.80	28.50			.25
3240	3.08	.72	1.96	9.70	16.60	30.00			.25
3250	3.07	.72	1.97	10.20	17.60	32.00			.25
3260	3.06	.72	1.99	10.70	18.60	34.50			.25
3270	3.05	.73	2.01	11.20	20.00	37.50			.25
3280	3.04	.73	2.02	11.80	21.20	41.00			.25
3290	3.03	.73	2.05	12.60	22.60	45.00			.25
3300	3.03	.74	2.08	13.30	24.50	53.00			.25
3310	3.02	.75	2.12	14.30	26.70	71.00			.25
3320	3.01	.76	2.15	15.30	29.20	90.00			.25
3330	3.00	.77	2.20	16.40	32.00	95.00			.25
3340	2.99	.79	2.24	17.10	34.80	98.00			.25
3350	2.98	.81	2.30	18.00	38.00	100.00			.25

Table I (Con't)

FINE STRUCTURE PARAMETERS FOR CO2 (THETA = 960.)
2.7 MICRON BAND
1/DO (CM.)

1/CM	MICRON	300 K	600 K	1200 K	1500 K	1800 K	2400 K	3000 K	EPSLON
3360	2.97	.83	2.37	18.30	41.50	104.00			.25
3370	2.96	.85	2.47	18.80	45.00	107.00			.25
3380	2.95	.87	2.57	19.10	45.50	113.00			.25
3390	2.94	.89	2.68	19.20	43.50	118.00			.25
3400	2.94	.92	2.80	19.00	40.00	120.00			.25
3410	2.93	.95	2.96	18.10	35.00	110.00			.25
3420	2.92	.98	3.13	17.00	30.00	70.00			.25
3430	2.91	1.02	3.32	15.40	25.00	44.00			.25
3440	2.90	1.06	3.55	13.70	20.00	31.50			.25
3450	2.89	1.10	3.80	12.00	16.30	23.50			.25
3460	2.89	1.15	4.05	10.50	13.30	17.40			.25
3470	2.88	1.20	4.37	9.30	11.00	13.30			.25
3480	2.87	1.26	4.65	8.10	9.10	10.50			.25
3490	2.86	1.33	4.68	7.00	7.60	8.50			.25
3500	2.85	1.41	4.55	6.10	6.60	7.20			.25
3510	2.84	1.50	4.30	5.40	5.70	6.40			.25
3520	2.84	1.62	4.00	4.70	5.10	5.50			.25
3530	2.83	1.80	3.60	4.20	4.50	4.70			.25
3540	2.82	1.86	3.15	3.80	4.10	4.30			.25
3550	2.81	1.70	2.70	3.50	3.70	3.90			.25
3560	2.80	1.48	2.25	3.30	3.50	3.65			.25
3570	2.80	1.24	1.84	3.55	3.35	3.65			.25
3580	2.79	1.00	1.27	3.45	3.30	3.85			.25
3590	2.78	.76	.91	2.45	3.25	4.50			.50
3600	2.77	.56	.70	2.10	3.20	5.70			.50
3610	2.77	.44	.54	2.50	3.35	7.50			.50
3620	2.76	.40	.35	3.20	4.30	10.50			.50
3630	2.75	.39	.27	3.65	6.50	14.80			.50

Table I (Con't)

FINE STRUCTURE PARAMETERS FOR CO2 (THETA = 960.)
2.7 MICRON BAND
1/DO (CM.)

1/CM	MICRON	300 K	600 K	1200 K	1500 K	1800 K	2400 K	3000 K	EPSLON
3640	2.74	.80	.40	3.95	8.10	19.80			.50
3650	2.73	.89	1.10	4.20	8.40	21.00			.50
3660	2.73	.81	1.40	4.70	8.30	19.80			.50
3670	2.72	.43	1.31	3.90	8.10	17.40			.50
3680	2.71	.44	1.20	3.75	7.70	15.20			.50
3690	2.71	.50	1.15	4.05	7.20	13.00			.50
3700	2.70	.58	1.20	4.30	6.70	11.20			.50
3710	2.69	.69	1.30	4.10	6.10	9.70			.50
3720	2.68	.83	1.45	3.80	5.60	8.40			.50
3730	2.68	1.09	1.60	3.50	5.10	7.30			.50
3740	2.67	1.55	1.72	3.30	4.60	6.30			.50
3750	2.66	2.30	1.80	3.10	4.10	5.40			.10
3760	2.65	2.40	1.67	2.40	3.70	4.70			.10
3770	2.65	1.80	1.50	1.45	3.25	4.00			.10

Table II

FINE STRUCTURE PARAMETERS FOR CO2 (THETA = INFINITY)
4.3 MICRON BAND
1/DLR (CM.)

1/CM	MICRON	300 K	600 K	1200 K	1500 K	1800 K	2400 K	3000 K
2000	5.00	.2553E 01	.1449E 02	.1844E 03	.4008E 03	.8727E 03	.2820E 04	.7015E 04
2010	4.97	.2553E 01	.1449E 02	.1844E 03	.4008E 03	.8727E 03	.2810E 04	.6865E 04
2020	4.95	.2553E 01	.1449E 02	.1844E 03	.4008E 03	.8727E 03	.2797E 04	.6492E 04
2030	4.92	.2553E 01	.1449E 02	.1844E 03	.4008E 03	.8727E 03	.2774E 04	.6119E 04
2040	4.90	.2553E 01	.1449E 02	.1844E 03	.4008E 03	.8727E 03	.2760E 04	.5746E 04
2050	4.87	.2553E 01	.1449E 02	.1844E 03	.4008E 03	.8727E 03	.2751E 04	.5373E 04
2060	4.85	.2553E 01	.1449E 02	.1844E 03	.4008E 03	.8727E 03	.2715E 04	.5000E 04
2070	4.83	.2553E 01	.1449E 02	.1844E 03	.4008E 03	.8727E 03	.2683E 04	.4552E 04
2080	4.80	.2553E 01	.1449E 02	.1844E 03	.4008E 03	.8727E 03	.2638E 04	.4253E 04
2090	4.78	.2553E 01	.1449E 02	.1844E 03	.4008E 03	.8727E 03	.2565E 04	.3880E 04
2100	4.76	.2553E 01	.1449E 02	.1844E 03	.4008E 03	.8603E 03	.2501E 04	.3582E 04
2110	4.73	.2553E 01	.1449E 02	.1844E 03	.4008E 03	.8528E 03	.2342E 04	.3283E 04
2120	4.71	.2553E 01	.1449E 02	.1844E 03	.4008E 03	.8353E 03	.2205E 04	.3059E 04
2130	4.69	.2553E 01	.1449E 02	.1844E 03	.4008E 03	.8104E 03	.2046E 04	.2798E 04
2140	4.67	.2553E 01	.1449E 02	.1844E 03	.4008E 03	.7780E 03	.1864E 04	.2537E 04
2150	4.65	.2553E 01	.1449E 02	.1844E 03	.4008E 03	.7480E 03	.1705E 04	.2313E 04
2160	4.62	.2553E 01	.1449E 02	.1809E 03	.3974E 03	.7057E 03	.1582E 04	.2052E 04
2170	4.60	.2553E 01	.1449E 02	.1763E 03	.3921E 03	.6682E 03	.1387E 04	.1828E 04
2180	4.58	.2553E 01	.1449E 02	.1728E 03	.3869E 03	.6308E 03	.1228E 04	.1611E 04
2190	4.56	.2553E 01	.1449E 02	.1682E 03	.3747E 03	.5934E 03	.1091E 04	.1432E 04
2200	4.54	.2553E 01	.1449E 02	.1613E 03	.3538E 03	.5486E 03	.9551E 03	.1268E 04
2210	4.52	.2553E 01	.1430E 02	.1521E 03	.3259E 03	.4987E 03	.8551E 03	.1104E 04
2220	4.50	.2553E 01	.1423E 02	.1417E 03	.2788E 03	.4314E 03	.7732E 03	.9701E 03
2230	4.48	.2553E 01	.1411E 02	.1302E 03	.2353E 03	.3740E 03	.6777E 03	.8358E 03
2240	4.46	.2553E 01	.1392E 02	.1164E 03	.1969E 03	.3241E 03	.5503E 03	.7313E 03
2250	4.44	.2553E 01	.1373E 02	.1048E 03	.1743E 03	.2792E 03	.4548E 03	.6343E 03
2260	4.42	.2553E 01	.1327E 02	.9221E 02	.1568E 03	.2493E 03	.4366E 03	.5522E 03
2270	4.40	.2553E 01	.1239E 02	.8068E 02	.1464E 03	.2219E 03	.4093E 03	.4627E 03

Table II (Con't)

FINE STRUCTURE PARAMETERS FOR CO2 (THETA = INFINITY)
4.3 MICRON BAND
1/DLR (CM.)

1/CM	MICRON	300 K	600 K	1200 K	1500 K	1800 K	2400 K	3000 K
2280	4.38	.2468E 01	.1106E 02	.6915E 02	.1342E 03	.1845E 03	.3320E 03	.3656E 03
2290	4.36	.2383E 01	.8965E 01	.5878E 02	.1167E 03	.1446E 03	.2319E 03	.2612E 03
2300	4.34	.2293E 01	.7826E 01	.8447E 02	.1091E 03	.2201E 03	.3408E 03	.4152E 03
2310	4.32	.1910E 01	.6521E 01	.6490E 02	.9376E 02	.1310E 03	.2236E 03	.2453E 03
2320	4.31	.1528E 01	.5739E 01	.4635E 02	.6183E 02	.8912E 02	.1278E 03	.1509E 03
2330	4.29	.1203E 01	.5739E 01	.3708E 02	.6478E 02	.6815E 02	.8841E 02	.1075E 03
2340	4.27	.1165E 01	.7304E 01	.3502E 02	.5114E 02	.6291E 02	.9054E 02	.1056E 03
2350	4.25	.2849E 01	.8005E 01	.2347E 02	.3430E 02	.3721E 02	.4863E 02	.5602E 02
2360	4.23	.1313E 01	.4618E 01	.1613E 02	.2017E 02	.2259E 02	.3171E 02	.3423E 02
2370	4.21	.1090E 01	.2413E 01	.7701E 01	.1156E 02	.1061E 02	.9790E 01	.9484E 01
2380	4.20	.1099E 01	.1763E 01	.3394E 01	.3380 E 01	.3319E 01	.3912E 01	.3131E 01
2390	4.18	.1460E 01	.1473E 01	.1469E 01	.1470 E 01	.1508E 01	.1906E 01	.1753E 01

Table II (Con't)

FINE STRUCTURE PARAMETERS FOR CO2 (THETA = INFINITY)
2.7 MICRON BAND
1/DLR (CM.)

1/CM	MICRON	300 K	600 K	1200 K	1500 K	1800 K	2400 K	3000 K
3080	3.24	.1225E 01	.7248E 01	.9221E 02	.2440E 03	.6234E 03		
3090	3.23	.1225E 01	.7248E 01	.9221E 02	.2440E 03	.6234E 03		
3100	3.22	.1225E 01	.7248E 01	.9221E 02	.2440E 03	.6234E 03		
3110	3.21	.1225E 01	.7248E 01	.9221E 02	.2440E 03	.6234E 03		
3120	3.20	.1225E 01	.7248E 01	.9221E 02	.2440E 03	.6234E 03		
3130	3.19	.1225E 01	.7248E 01	.9221E 02	.2440E 03	.6234E 03		
3140	3.18	.1225E 01	.7248E 01	.9221E 02	.2440E 03	.6234E 03		
3150	3.17	.1225E 01	.7248E 01	.9221E 02	.2440E 03	.6234E 03		
3160	3.16	.1225E 01	.7287E 01	.9336E 02	.2440E 03	.6234E 03		
3170	3.15	.1225E 01	.7287E 01	.9393E 02	.2457E 03	.6234E 03		
3180	3.14	.1225E 01	.7325E 01	.9451E 02	.2475E 03	.6234E 03		
3190	3.13	.1225E 01	.7325E 01	.9566E 02	.2527E 03	.6283E 03		
3200	3.12	.1225E 01	.7363E 01	.9797E 02	.2562E 03	.6433E 03		
3210	3.11	.1225E 01	.7363E 01	.1002E 03	.2614E 03	.6583E 03		
3220	3.10	.1225E 01	.7401E 01	.1025E 03	.2666E 03	.6782E 03		
3230	3.09	.1225E 01	.7439E 01	.1071E 03	.2753E 03	.7106E 03		
3240	3.08	.1225E 01	.7477E 01	.1118E 03	.2893E 03	.7480E 03		
3250	3.07	.1225E 01	.7516E 01	.1175E 03	.3067E 03	.7979E 03		
3260	3.06	.1225E 01	.7592E 01	.1233E 03	.3241E 03	.8603E 03		
3270	3.05	.1234E 01	.7668E 01	.1290E 03	.3486E 03	.9351E 03		
3280	3.04	.1237E 01	.7706E 01	.1360E 03	.3695E 03	.1022E 04		
3290	3.03	.1242E 01	.7821E 01	.1452E 03	.3974E 03	.1122E 04		
3300	3.03	.1254E 01	.7935E 01	.1532E 03	.4270E 03	.1321E 04		
3310	3.02	.1270E 01	.8088E 01	.1648E 03	.4653E 03	.1770E 04		
3320	3.01	.1285E 01	.8202E 01	.1763E 03	.5089E 03	.2244E 04		
3330	3.00	.1310E 01	.8393E 01	.1890E 03	.5577E 03	.2368E 04		
3340	2.99	.1344E 01	.8546E 01	.1970E 03	.6065E 03	.2443E 04		
3350	2.98	.1370E 01	.8775E 01	.2074E 03	.6623E 03	.2493E 04		

Table II (Con't)

FINE STRUCTURE PARAMETERS FOR CO2 (THETA = INFINITY)
2.7 MICRON BAND
1/DLR (CM.)

1/CM	MICRON	300 K	600 K	1200 K	1500 K	1800 K	2400 K	3000 K
3360	2.97	.1404E 01	.9042E 01	.2109E 03	.7233E 03	.2593E 04		
3370	2.96	.1438E 01	.9423E 01	.2166E 03	.7843E 03	.2668E 04		
3380	2.95	.1472E 01	.9805E 01	.2201E 03	.7930E 03	.2817E 04		
3390	2.94	.1506E 01	.1022E 02	.2213E 03	.7582E 03	.2942E 04		
3400	2.94	.1557E 01	.1068E 02	.2189E 03	.6972E 03	.2992E 04		
3410	2.93	.1608E 01	.1129E 02	.2086E 03	.6100E 03	.2743E 04		
3420	2.92	.1663E 01	.1194E 02	.1959E 03	.5229E 03	.1745E 04		
3430	2.91	.1736E 01	.1266E 02	.1775E 03	.4357E 03	.1097E 04		
3440	2.90	.1804E 01	.1354E 02	.1579E 03	.3486E 03	.7854E 03		
3450	2.89	.1872E 01	.1449E 02	.1383E 03	.2841E 03	.5860E 03		
3460	2.89	.1957E 01	.1545E 02	.1210E 03	.2318E 03	.4338E 03		
3470	2.88	.2042E 01	.1667E 02	.1071E 03	.1917E 03	.3316E 03		
3480	2.87	.2145E 01	.1774E 02	.9336E 02	.1586E 03	.2618E 03		
3490	2.86	.2264E 01	.1785E 02	.8068E 02	.1324E 03	.2119E 03		
3500	2.85	.2400E 01	.1735E 02	.7031E 02	.1150E 03	.1795E 03		
3510	2.84	.2553E 01	.1640E 02	.6224E 02	.9935E 02	.1595E 03		
3520	2.84	.2757E 01	.1526E 02	.5417E 02	.8889E 02	.1371E 03		
3530	2.83	.3064E 01	.1373E 02	.4841E 02	.7843E 02	.1172E 03		
3540	2.82	.3166E 01	.1201E 02	.4379E 02	.7146E 02	.1072E 03		
3550	2.81	.2894E 01	.1030E 02	.4034E 02	.6449E 02	.9725E 02		
3560	2.80	.2519E 01	.8584E 01	.3803E 02	.6100E 02	.9101E 02		
3570	2.80	.2111E 01	.7020E 01	.4091E 02	.5839E 02	.9101E 02		
3580	2.79	.1702E 01	.4845E 01	.3976E 02	.5751E 02	.9600E 02		
3590	2.78	.1452E 01	.4748E 01	.5048E 02	.1108E 03	.2359E 03		
3600	2.77	.1070E 01	.3652E 01	.4326E 02	.1091E 03	.2988E 03		
3610	2.77	.8408E 00	.2817E 01	.5151E 02	.1142E 03	.3931E 03		
3620	2.76	.7643E 00	.1826E 01	.6593E 02	.1466E 03	.5504E 03		
3630	2.75	.7452E 00	.1408E 01	.7520E 02	.2216E 03	.7759E 03		

Table II (Con't)

FINE STRUCTURE PARAMETERS FOR CO2 (THETA = INFINITY)
2.7 MICRON BAND
1/DLR (CM.)

1/CM	MICRON	300 K	600 K	1200 K	1500 K	1800 K	2400 K	3000 K
3640	2.74	.1528E 01	.2087E 01	.8138E 02	.2761E 03	.1038E 04		
3650	2.73	.1700E 01	.5739E 01	.8653E 02	.2864E 03	.1100E 04		
3660	2.73	.1547E 01	.7304E 01	.9683E 02	.2830E 03	.1038E 04		
3670	2.72	.8121E 00	.6835E 01	.8035E 02	.2761E 03	.9122E 03		
3680	2.71	.8312E 00	.6261E 01	.7726E 02	.2625E 03	.7968E 03		
3690	2.71	.9459E 00	.6000E 01	.8344E 02	.2454E 03	.6815E 03		
3700	2.70	.1108E 01	.6261E 01	.8859E 02	.2284E 03	.5871E 03		
3710	2.69	.1318E 01	.6782E 01	.8447E 02	.2079E 03	.5085E 03		
3720	2.66	.1576E 01	.7565E 01	.7829E 02	.1909E 03	.4403E 03		
3730	2.68	.2082E 01	.8348E 01	.7211E 02	.1738E 03	.3827E 03		
3740	2.67	.2962E 01	.8974E 01	.6799E 02	.1568E 03	.3302E 03		
3750	2.66	.3641E 01	.5542E 01	.2274E 02	.4136E 02	.7176E 02		
3760	2.65	.3799E 01	.5141E 01	.1760E 02	.3733E 02	.6246E 02		
3770	2.65	.2849E 01	.4618E 01	.1063E 02	.3278E 02	.5315E 02		

TABLE VIII. ABSORPTION COEFFICIENTS FOR CARBON (SQ. CM/GM)

TEMPERATURE IN DEGREES KELVIN

WAVENUMBER IN RECIPROCAL CM

TEMP.---	300.	600.	1000.	1500.	2000.	2500.	3000.
WAVENO.							
1000.00	.1909E 04	.1769E 04	.1599E 04	.1269E 04	.9699E 03	.7599E 03	.6189E 03
1428.60	.3228E 04	.3085E 04	.2928E 04	.2428E 04	.1928E 04	.1542E 04	.1257E 04
1666.67	.3933E 04	.3833E 04	.3666E 04	.3166E 04	.2583E 04	.2083E 04	.1699E 04
2000.00	.4899E 04	.4799E 04	.4699E 04	.4259E 04	.3579E 04	.2919E 04	.2439E 04
2500.00	.6099E 04	.6149E 04	.6250E 04	.5899E 04	.5249E 04	.4424E 04	.3750E 04
3333.33	.7633E 04	.7999E 04	.8366E 04	.8499E 04	.8166E 04	.7500E 04	.6566E 04
4000.00	.8599E 04	.9199E 04	.9799E 04	.1051E 05	.1055E 05	.1007E 05	.9199E 04
5000.00	.1000E 05	.1074E 05	.1149E 05	.1299E 05	.1399E 05	.1424E 05	.1375E 05
6666.67	.1226E 05	.1313E 05	.1413E 05	.1673E 05	.1926E 05	.2099E 05	.2199E 05
8333.33	.1458E 05	.1574E 05	.1666E 05	.2008E 05	.2375E 05	.2749E 05	.3008E 05
10000.00	.1750E 05	.1879E 05	.2000E 05	.2349E 05	.2799E 05	.3309E 05	.3750E 05
11111.10	.1999E 05	.2111E 05	.2244E 05	.2611E 05	.3055E 05	.3655E 05	.4144E 05
14286.00	.2714E 05	.2857E 05	.3014E 05	.3428E 05	.3914E 05	.4499E 05	.5142E 05
20000.00	.4199E 05	.4319E 05	.4539E 05	.5019E 05	.5599E 05	.6219E 05	.6699E 05